ORIGINAL RESEARCH

Activin Receptor-Like Kinase 4 Haplodeficiency Mitigates Arrhythmogenic Atrial Remodeling and Vulnerability to Atrial Fibrillation in Cardiac Pathological Hypertrophy

Qian Wang, MD;* Yihe Chen, MD;* Daoliang Zhang, MD; Changyi Li, MD; Xiaoqing Chen, MD; Jianwen Hou, MD; Yudong Fei, MD; Yuepeng Wang, PhD; Yigang Li, MD

***Background*—**Activin receptor-like kinase 4 (ALK4) is highly expressed in mammal heart. Atrial fibrillation (AF) is closely related to ventricular pressure overload. Because pressure overload increases atrial pressure and leads to atrial remodeling, it would be informative to know whether ALK4 exerts potential effects on atrial remodeling and AF vulnerability in a pressure-overload model.

***Methods and Results*—**Wild-type littermates and ALK4$^{+/-}$ mice were subjected to abdominal aortic constriction or a sham operation. After 4 or 8 weeks, echocardiographic and hemodynamic measurements were performed, and inducibility of AF was tested. The hearts were divided into atria and ventricles and then were fixed in formalin for staining, or they were weighted and snap-frozen for quantitative real-time polymerase chain reaction and Western blot analysis. Compared with wild-type littermates, ALK4$^{+/-}$ mice demonstrated a similar extent of atrial hypertrophy but significantly suppressed atrial fibrosis at 8 weeks post–abdominal aortic constriction. ALK4 haplodeficiency partially blocked abdominal aortic constriction–induced upregulation of monocyte chemotactic protein 1 and interleukin-6, and the increased chemotaxin of macrophages. ALK4 haplodeficiency also blunted a reduction of connexin 40 and redistribution of connexin 43 from the intercalated disk to the lateral membranes, thereby improving localized conduction abnormalities. Meanwhile, ALK4 haplodeficiency inhibited abdominal aortic constriction–induced decreased I_{Na}, $I_{Ca\text{-}L}$ and I_{K1} densities as well as the accompanying action potential duration shortening. Mechanistically, ALK4 haploinsufficiency resulted in the suppression of Smad2/3 activity in this model.

***Conclusions*—**Our results demonstrate that ALK4 haplodeficiency ameliorates atrial remodeling and vulnerability to AF in a pressure-overload model through inactivation of the Smad2/3 pathway, suggesting that ALK4 might be a potential therapeutic target in combating pressure overload–induced AF. **(*J Am Heart Assoc*. 2018;7:e008842. DOI: 10.1161/JAHA.118.008842.)**

Key Words: ALK4 • atrial fibrillation • cardiac hypertrophy • Smad2/3 • structural and electrical remodeling

Atrial fibrillation (AF) is the most prevalent arrhythmia encountered in the clinical setting; it increases the risk of embolic stroke, heart failure, and overall mortality.[1] AF is associated with structural and electrical remodeling, including atrial fibrosis, atrial dilatation, cellular hypertrophy, variation in ion channel expression, and inflammation. Among these, structural remodeling characterized by atrial fibrosis and dilatation enhances the AF vulnerability by reentry activity.[2] Electrical remodeling is another essential pathomechanism of AF. Previous studies demonstrated that expression modulation of several ion channels including CACNA1C, SCN5A, KCNQ1, KCNH2, and junctional complexes including connexin 40 (Cx40) and connexin 43 (Cx43) were critically involved in the development of AF through regulation of action potential duration (APD) or conduction velocity in atrium.[3]

As is known, the vast majority of AF occurs in the circumference of underlying diseases including hypertension, heart failure, cardiomyopathy, or valve diseases, and among these hypertension is the most prevalent comorbidity.[4,5] Currently, hypertension is estimated to be responsible for 22% of incident AF cases[6] and is considered the most widespread and modifiable risk factor for AF.[4] The increased afterload may lead to increased risk of AF and worsen outcomes of AF

From the Department of Cardiology, Xinhua Hospital, School of Medicine (Q.W., Y.C., C.L., J.H., Y.F., Y.W., Y.L.), and Department of Cardiology, Shanghai Chest Hospital (D.Z.), Shanghai Jiao Tong University, Shanghai, China; Department of Cardiology, Shanghai General Hospital, Shanghai Jiao Tong University School of Medicine, Shanghai, China (X.C.).

Accompanying Tables S1, S2 and Figures S1 through S4 are available at https://www.ahajournals.org/doi/suppl/10.1161/JAHA.118.008842

*Dr Qian Wang and Dr Yihe Chen contributed equally to this work.

Correspondence to: Yigang Li, MD, Department of Cardiology, Xinhua Hospital, School of Medicine, Shanghai Jiao Tong University, 1665 Kongjiang Road, Shanghai 200092, China. E-mail liyigang@xinhuamed.com.cn

Received February 5, 2018; accepted June 12, 2018.

Clinical Perspective

What Is New?

- Activin receptor-like kinase 4 haplodeficiency improved the arrhythmogenic substrate in atria by reduced structural remodeling, ion-channel remodeling, and inflammation, especially the chemotaxis of macrophages caused by aortic constriction, and finally attenuated vulnerability to atrial fibrillation in hypertrophic hearts.

What Are the Clinical Implications?

- Activin receptor-like kinase 4/Smad2/3 pathway activation is related to aortic constriction–induced atrial fibrillation.
- An activin receptor-like kinase 4 inhibitor may act as a promising therapeutic target for the upstream prevention of atrial fibrillation in pressure-overloaded hearts.

via left ventricular (LV) diastolic dysfunction, left atrial (LA) overload, and remodeling.[7] In our study we chose the suitable animal model that could best resemble AF in human hypertensive pathophysiological conditions to uncover potential molecular mechanisms of AF that have not yet been studied in patients with AF. To date, dozens of animal models relating to AF have been described in the literature.[3] Most of these animal models are developed in large animals such as the dog and goat or in small animals such as the mouse. These animal models can be simply divided into 3 broad categories[3]: those with atrial conduction abnormalities that act as a reentry substrate, those with electrophysiological abnormalities that affect atrial repolarization and facilitate reentry, and those with a predisposition to focal ectopic firing. Most of these models have cardiomyopathic phenotypes with atrial structural or electrical remodeling in common. Among these, our previous study had focused on the setting of angiotensin II–induced atrial fibrosis and vulnerability to AF.[8] Although angiotensin II, a key component of the renin-angiotensin system, also induces hypertension and cardiac hypertrophy, the model only considers the effect of angiotensin II, a powerful but single factor, on the heart. When the osmotic minipump was implanted for subcutaneous infusion of angiotensin II, the angiotensin II instantly worked on the heart. However, some patients with AF and underlying hypertension showed no increase of angiotensin II concentration in serum or atria. Thus, this model could not fully mimic AF in human hypertensive pathophysiological conditions. Cardiac hypertrophy induced by aortic constriction represents a similar outcome of LV hypertrophic processes observed in patients with hypertension and is a result of many complex factors such as pressure overload, neuroendocrine changes, and the corresponding renin-angiotensin system activation. Compared with the model of angiotensin II–induced AF, the model of aortic constriction–induced AF shows similar pathological process such as a hypertrophic condition underlying hypertension, but this model also shows different pathophysiological processes that more closely resemble AF in human hypertensive pathophysiological conditions.[1] So unlike the previous study,[8] this study explored atrial structural and electrical remodeling in the pressure-overloaded heart.

Activin receptor-like kinase 4 (ALK4), also known as ACVR1B, is a transmembrane serine/threonine kinase activin type-I receptor and is highly expressed in the mammal heart. ALK4 forms an activin receptor complex with activin type-II receptor to transduce activin signal from the cell surface to the cytoplasm,[8-11] thus regulating physiological and pathological processes including embryogenesis,[12] tissue homeostasis,[13] wound healing,[14] extracellular matrix production,[15] immunosuppression, and carcinogenesis.[16,17] We recently focused on exploring the role of ALK4 in different cardiovascular diseases. We have demonstrated that ALK4 was upregulated in ventricles of pressure-overloaded hearts,[18] in the infarct border zone after myocardial infarction,[19] and in the atrium post–angiotensin II infusion,[8] whereas ALK4 haplodeficiency attenuated pressure overload– and myocardial infarction–induced ventricular fibrosis and angiotensin II–induced atrial fibrosis.[8,18,19] However, whether ALK4 exerts effects on the progression of atrial remodeling and its association with vulnerability to AF in the model of ventricular pressure overload remain unknown. The experiments here were undertaken to test the hypothesis that ALK4 haplodeficiency could counteract the adverse atrial structural and/or electrical remodeling and finally mitigate the vulnerability to atrial fibrillation associated with pathological hypertrophy.

In the present study we explored the role of ALK4 in the progression of atrial remodeling in the mouse model of ventricular pressure overload, which somehow mimics the AF pathology associated with hypertension. Our data revealed that ALK4 haplodeficiency ameliorated structural and electrical remodeling as well as inflammation in atrium and finally reduced the vulnerability to AF in the mice subjected to aortic banding. These results enriched the protective role of ALK4 haplodeficiency in the pathogenesis of diverse cardiovascular diseases and hinted that targeting ALK4 might be a new potential therapeutic option for treating pressure overload–induced atrial remodeling and reducing pressure overload–induced increased vulnerability to AF.

Materials and Methods

Data Availability

The authors confirm that the data, analytic methods, and study materials will be available to other researchers for the purposes of reproducing the results or replicating the

procedure. Material will be available from Shanghai Xinhua Hospital affiliated to Shanghai Jiao Tong University School of Medicine, which is responsible for maintaining availability on request to the corresponding author.

Ethical Statement

The study was approved by the ethics committee of Shanghai Xinhua Hospital affiliated with Shanghai Jiao Tong University School of Medicine. The study involving human LA samples was approved by the Ethics Committee of Xinhua Hospital affiliated with Shanghai Jiao Tong University School of Medicine. All animal experiments were performed in accordance with the National Institutes of Health Guidelines for the care and use of laboratory animals.

Human LA Samples

Written consent was obtained from each enrolled patient. LA samples were collected from the patients undergoing surgery due to mitral insufficiency in Xinhua Hospital. Patients with chronic heart failure, coronary heart disease, cardiomyopathy, hyperthyroidism, chronic pulmonary heart disease, or diabetes mellitus were excluded. According to the presence or absence of AF, patients were divided into the permanent AF group (n=10) and the sinus rhythm (SR) group (n=10). The AF group was then divided into AF patients with underlying hypertension (n=5) and those devoid of hypertension (n=5). The baseline characteristics of enrolled patients are listed in Table S1.

ALK4 Haplodeficiency Mice and AAC Model

ALK4 haplodeficiency ($ALK4^{+/-}$) mice and wild-type (WT) littermates were generated as described before.[18] All mice were in the C57BL/6J background. Eight-week-old male mice were randomly divided into 4 equal groups (n=12 in each group): (1) WT littermates undergoing a sham operation; (2) WT littermates undergoing an abdominal aortic constriction (AAC) operation; (3) $ALK4^{+/-}$ mice undergoing a sham operation; (4) $ALK4^{+/-}$ mice undergoing an AAC operation. Briefly, mice assigned to AAC groups were anesthetized with 2% isoflurane inhalation. A 7-0 silk suture was placed around the suprarenal abdominal aorta and tied around a 27-gauge desharpened needle, which was then subsequently removed.[1,20] For sham operations, the suture was placed around the suprarenal abdominal aorta without ligation.

Intraperitoneal Administration of ALK4 Inhibitor SB-431542

Eight-week-old male WT littermates were subjected to either AAC or a sham operation as mentioned above. After the animal surgery, ALK4 inhibitor SB-431542 (1 μmol/L solution, 100 μL/mouse; Selleckchem, Houston, TX) or vehicle alone was intraperitoneally administered on the first and third days after the models were established successfully and was repeated every 4 days for a further 8 weeks.[8,21]

Osmotic Minipump Implantation of Smad3 Inhibitor SIS3

Eight-week-old male WT littermates were subjected either to AAC or a sham operation as mentioned above. After the animal surgery, an Alzet osmotic minipump was implanted for subcutaneous delivery of Smad3 inhibitor SIS3 (2.5 mg/kg per day) for 8 weeks.[22] At the end of the experiments, a burst of programmed electrical stimulation was performed to evaluate the inducibility of AF.

Echocardiographic Measurements

At 4 or 8 weeks post-AAC or sham operation, in vivo cardiac dimensions and functional parameters were assessed using transthoracic echocardiography (Vivid 7, GE Medical, Milwaukee, WI). Mice were anesthetized as described previously,[8] and body temperature was maintained at 37°C by placing the mice on a heating pad. Parasternal short-axis views were used to record M-mode tracings at the LV midpapillary level to measure LV dimensions, including interventricular septum, LV posterior wall, LV internal diameter, and ejection fraction.[18] Apical 4-chamber view was used to assess the size of the LA. LA length was measured at end-systole from the tip of the mitral valve closure to the base of the LA.[8]

Hemodynamic Measurements

For hemodynamic measurements, a 1.4F Millar pressure catheter (SPR-839; Millar Instruments, Houston, TX) was introduced through the right carotid artery into the LV, and LV end-diastolic pressure was recorded.[18]

Intracardiac Electrophysiological Recordings

Mice were anesthetized with 2% isoflurane. To maintain body temperature at 37°C, the mice were placed on a heated pad. A 1.1F electrode catheter (Scisense, London, ON, Canada) was advanced through the right jugular vein into the right atrium. A burst of programmed electrical stimulation was performed to evaluate the inducibility of AF. Each burst stimulation lasted for 5 seconds, starting from the cycle length of 50 milliseconds, decreasing to 48, 46, and 44 milliseconds and ultimately reduced to 10 milliseconds.[8] Following these successive bursts, the incidence of AF and AF duration were analyzed; these were separately defined as

rapid and irregular atrial excitation lasting more than 1 second, and the time from the end of burst pacing to the first P wave was measured after rapid irregular atrial rhythm. Meanwhile, a surface 6-lead ECG was recorded and monitored throughout the experimental procedures. After echocardiography and intracardiac electrophysiological investigation had been performed, mice were anesthetized by abdominal injection of sodium phenobarbital (100 mg/kg) and euthanized by swift decapitation according to NIH guidelines.[19,23] Then the heart and tibia were extracted separately.

Histology

Hearts were divided into atria and ventricles, fixed in 10% formalin overnight, and embedded in paraffin. Subsequently, the LA and the ventricles were sectioned transversely at 5 μm. Ventricular sections were stained with hematoxylin and eosin for histopathology. LA and ventricular sections were stained with picrosirius red to evaluate fibrotic areas. Based on the picrosirius red–stained sections, the LA or LV collagen volume fraction was calculated as the area stained by picrosirius red divided by the total area. The cross-sectional area of atrial or ventricular myocytes was determined using a quantitative digital image analysis system (Image Pro Plus 6.0; Media Cybernetics, Rockville, MD) from images captured from FITC-conjugated wheat germ agglutinin (Sigma, St. Louis, MO)-stained LA or ventricular sections. More than 100 atrial or ventricular myocytes in the sections were outlined in each group.

Immunohistochemistry and Immunofluorescence Staining

Here, only the LA samples were used for immunohistochemistry or immunofluorescence staining. For immunohistochemistry staining, LA sections were stained with antibody against Cx43 (1:200; Thermo Fisher Scientific, Waltham, MA) as previously described.[19] Images were captured with an Olympus microscope attached to a computerized imaging system. For immunofluorescence staining, LA sections were stained with antibody against α-smooth muscle actin (α-SMA, 1:200; Abcam, Cambridge, UK) and Cx40 (1:200, Thermo Fisher Scientific). The nuclei were labeled with 4′,6-diamidino-2-phenylindole (DAPI, 1:1; Life Technologies, Carsbad, CA).[18] Fluorescent signals were captured with a fluorescence microscope or a confocal microscope. All images were analyzed by Image-Pro Plus 6.0.

Isolation and Culture of Atrial Fibroblasts and Peritoneal Macrophages

Isolation of primary atrial fibroblasts was performed as previously described.[8,24] Briefly, for each batch, 10 to 12 8-week-old $ALK4^{+/-}$ mice or WT littermates post-AAC for 8 weeks and their corresponding sham groups were euthanized as mentioned above. The hearts were rapidly harvested and washed in cold PBS. The atrium was cut into pieces with a tissue chopper and then was digested with 1% collagenase II (Worthington Biochemical, Lakewood, NJ) at 37°C for 30 minutes. After being filtered and centrifugated at 310g for 5 minutes, the cells were resuspended and cultured in DMEM containing 10% fetal calf serum and 100 U/mL penicillin/streptomycin for 1.5 hours. After removal of the myocyte-enriched medium, fresh DMEM was then added to the preplated atrial fibroblasts. Cells between passages 2 to 4 were used for the study.

To collect the peritoneal macrophages of $ALK4^{+/-}$ mice or WT littermates post-AAC for 8 weeks and their corresponding sham group, at least 3 mice were injected intraperitoneally with 1 mL sterile 10% thioglycollate broth (Sigma). Three days later, the mouse abdomen was cleaned with 75% ethanol, a small incision was made with a sterile scalpel, and then the abdominal skin was removed to expose the peritoneum.[25] A 5-mL syringe with a 25 gauge needle was used to inject 4 mL PBS into the peritoneal cavity. After gentle massaging of the mouse abdomen, as much PBS as possible was recovered into a 15-mL tube. After centrifugation for 5 minutes at 4°C at 310*g* to pellet the cells, supernatant was discarded, and the cells were resuspended in Roswell Park Memorial Institute medium. After collection, macrophages were passaged for experiments the next day.

Isolation of Atrial Cardiomyocytes

$ALK4^{+/-}$ mice and WT littermates 8 weeks after sham or AAC surgery were heparinized (100 U intraperitoneally) and anesthetized using sodium pentobarbital (60 mg/kg intraperitoneally). The hearts were rapidly removed and connected to a Langendorff apparatus with a constant flow at a rate of 3 mL/min for retrograde perfusion through the aorta, at 37°C for 5 minutes of perfusion with Ca^{2+}-free Tyrode solution (mmol/L): NaCl 126; KCl 5.4; $MgCl_2$ 1; Na_2HPO_4 0.3; HEPES 10; glucose 10; pH adjusted to 7.4 with NaOH.[26] Then the hearts were further digested with the same solution containing collagenase type II (0.6 mg/mL, Worthington), 0.1% bovine serum albumin, and 0.04 mg/mL protease for another 5 to 10 minutes. The atrium was dissected and placed in a small vessel containing fresh enzyme solution as mentioned above for another 5 to 10 minutes. Finally, single atrial cardiomyocytes were separated by pipetting and were stored in a potassium buffer solution (mmol/L) (KOH 85; K-glutamate 50; taurine 20; KCl 30; $MgCl_2$ 1.0; EGTA 0.5; HEPES 10; and glucose 10, with pH adjusted to 7.4 with KOH) at 4°C until a patch-clamp recording was done.[27]

Cellular Electrophysiology Recording

All experiments were performed at 36°C to 37°C. Data were acquired using whole-cell recording technique (Axopatch 700B amplifier; Axon Instruments, Inc, Union City, CA) as described previously.[27] Briefly, cells were placed in a 1-mL chamber and superfused with external solution at 2 mL/min for 5 to 10 minutes before being clamped, and another 5 minutes was allowed to stabilize the parameters after the cell had been entered. For ionic current recordings, series resistance was electrically compensated to 70% to 80%.

For action potential (AP) recordings, isolated atrial myocytes were superfused with standard Tyrode solution. Patch pipettes with tip resistance of 2 to 3 MΩ were filled with pipette solution containing (mmol/L): K-aspartate 110; KCl 30; NaCl 5; HEPES 10; EGTA 0.1; MgATP 5; creatine phosphate 5; and cAMP 0.05, pH 7.2 with KOH. APs were elicited by 2-millisecond-duration, 1000- to 2000-pA rectangular pulses at a basic cycle length of 1 second. The last 10 steady-state APs were measured at 50% (APD_{50}) and 90% (APD_{90}) repolarization.[27]

To record I_{Na}, micropipettes with tip resistances of ≈1 to 2 MΩ were filled with internal solution containing (mmol/L): CsCl 133; TEACl 20; HEPES 5; EGTA 10; MgATP 5; and NaCl 5, pH adjusted to 7.3 with CsOH. The perfused solution was used, containing (mmol/L): CsCl 133; NaCl 5; HEPES 5; glucose 5; $MgCl_2$ 2; $CaCl_2$ 1.8; nifedipine 0.002, with PH of 7.3. I_{Na} was recorded during depolarization from a holding potential of −120 mV, to test potentials ranging from −70 to +60 mV in 5-mV steps for 40 milliseconds.[28]

To record $I_{Ca\text{-}L}$, atrial cardiomyocytes were perfused with a modified Tyrode solution in which KCl was replaced with equivalent CsCl, and TTX (10 μmol/L) was added to block I_{NaL}. The micropipettes with tip resistances of ≈2 to 4 MΩ were filled with solution containing (mmol/L): CsCl 20; Cs-aspartate 100; $MgCl_2$ 1; TEACl 20; EGTA 10; HEPES 10; and MgATP 5, pH adjusted to 7.20 with CsOH. $I_{Ca\text{-}L}$ was recorded using a series of 200-millisecond steps from −40 to +50 mV with an increment of 10 mV from a holding potential of −80 mV before a 100-millisecond prepulse to −40 mV.

To record I_{to}, the external solution and pipette solution were the same as those for AP recording; 300 μmol/L $CdCl_2$ and 10 μmol/L TTX were added in Tyrode solution to block $I_{Ca\text{-}L}$ and $I_{Na\text{-}L}$. The current was elicited by a series of 300-millisecond depolarizing steps from a holding potential of −40 mV to potentials ranging from −40 mV to +50 mV in 10-mV increments.

To record I_{K1}, external Na^+ in Tyrode solution was replaced by equimolar choline (126 nmol/L). 4-Aminopyridine (5 mmol/L), $CdCl_2$ (300 μmol/L), dofetilide (1 μmol/L), chromanol (10 μmol/L), and glibenclamide (1 μmol/L) were added in the external solution to block I_{to}, I_{Ca}, I_{Kr}, I_{ks}, and $I_{K\text{-}ATP}$. The pipette solution contained (mmol/L): KCl 140, $MgCl_2$ 1, KATP 5, EGTA 5, NaGTP 0.1, Na_2-creatine phosphate 3, and HEPES 10, pH adjusted to 7.2 with KOH. The current-voltage relationship was established using 400-millisecond depolarizing pulses from a holding potential of −40 mV to potentials ranging from −120 mV to 0 mV with 10-mV increments.[29] Current densities (pA/pF) were all obtained by normalizing the current amplitudes (pA) to membrane capacitance C_m (pF).

CCK-8 Assay

The proliferation of atrial fibroblasts was detected using a cell counting kit (CCK-8, Dojindo Molecular Technologies, Rockville, MD) assay. Atrial fibroblasts isolated from $ALK4^{+/-}$ mice and WT littermates undergoing sham surgery or AAC for 8 weeks were seeded in 96-well plates at a density of 3×10^3 cells/well. Experiments were detected in 5 replicate wells for each group. After cell culture for 0, 12, 24, and 48 hours, each well was supplemented with 10 μL CCK-8 solution (Dojindo Molecular Technologies) and incubated at 37°C for 2 hours. The optical density tested by a microplate reader (BioTek, Winooski, VT) was measured at 450 nm.

Transwell Assay

Atrial fibroblasts isolated from $ALK4^{+/-}$ mice and WT littermates 8 weeks after undergoing sham surgery or AAC were plated in the bottom chamber of a 24-well plate and incubated at 37°C with 5% CO_2 overnight. After being cultured in serum-free medium for 12 hours, fibroblasts were cultured for another 24 hours. At the same time, mouse peritoneal macrophages isolated from $ALK4^{+/-}$ mice and WT littermates 8 weeks after sham surgery prepared at a concentration of 1×10^5/mL were harvested and added into 8.0-μm-pore-size transwell inserts (Millipore, Burlington, MA). Twenty-four hours later, we performed staining with 0.25% crystal violet as described,[8] and 5 high-power fields (100×) were used to count the average number of migrated macrophages per field.

Western Blot Analysis

Frozen LA or LV tissues were homogenized and centrifuged using radioimmunoprecipitation assay lysis buffer and then underwent Western blot analysis as described.[8] LV tissues were used only to detect the expression of ALK4, and LA tissues were used to detect a wide range of proteins including ALK4, proliferation cellular nuclear antigen, α-SMA, Cx40, Cx43, p-Smad2/3, Smad2/3, p-ERK, ERK, p-JNK, JNK, p-p38, and p38. All of the protein expression levels were quantified and normalized to the GAPDH loading control. Primary antibodies were as follows: ALK4 (1:500; Proteintech Group, Inc, Chicago, IL); proliferation cellular nuclear antigen (1:1000, Abcam,

Cambridge, UK); α-SMA (1:1000; Abcam); Cx40 (1:600; Thermo Fisher Scientific, Waltham, MA); Cx43 (1:1000; Thermo Fisher Scientific); CTGF (1:1000; Abcam); p-Smad2 (1:500; Cell Signaling, Danvers, MA); p-Smad3 (1:1000; Cell Signaling); Smad2/3 (1:1000; Cell Signaling); ERK (1:1000; Cell Signaling); p-ERK (1:1000; Cell Signaling); JNK (1:1000; Cell Signaling); p-JNK (1:1000; Cell Signaling); p38 (1:1000; Cell Signaling); and p-p38 (1:1000; Cell Signaling).

Real-Time PCR

Total RNA was isolated from LA or LV tissue using TRIzol reagent (Invitrogen, Carlsbad, CA). cDNA was synthesized from 1000 ng of total RNA obtained from each sample using PrimeScript RT reagent kit (Takara, Kusatsu, Japan). Quantitative real-time polymerase chain reaction (RT-PCR) was performed with SYBR green (Takara) in 20-μL volumes to detect PCR products. Data were normalized to GAPDH for LA or LV samples and expressed as relative mRNA levels. Primer pairs for RT-PCR in this study are shown in Table S2.

Statistical Analysis

All results are represented as mean±SEM or percentage, and data analysis was performed by SPSS 19.0 software. Student t test was used to compare results between the 2 groups. One-way ANOVA analysis followed by a post hoc Tukey test or 2-way ANOVA analysis followed by an ad hoc Bonferroni test was performed for multiple-group comparisons. A value of $P<0.05$ was considered statistically significant.

Results

Expression of ALK4 is Upregulated in AF Human Atrium, With Higher ALK4 Expression in AF Human Atrium Underlying Hypertension

We have demonstrated that compared with patients with SR, patients with AF showed significantly higher ALK4 mRNA and protein expression.[8] It is worth noting that among AF patients, those with underlying hypertension showed higher ALK4 expression and accompanying increased diastolic interventricular septum thickness than those devoid of hypertension (Figure S1 and Table S1). The above data indicated that ALK4 might be involved in AF, especially in those with underlying hypertensive pathophysiological conditions.

Validation of the Model: Ventricular Remodeling Post-ACC

To elucidate the role of ALK4 in the development of atrial remodeling induced by pressure overload, we first conducted AAC, and the mice were examined at 4 or 8 weeks post-AAC. As expected, the heart weight, the LV gene expression associated with hypertrophy as well as the size of ventricular myocyte were all significantly elevated in WT littermates (Figure S2B through S2D and S2F), whereas the ejection fraction was dramatically reduced (Figure S3C) at 4 or 8 weeks post AAC, indicating the successful establishment of the AAC model. Next, we further explored the effect of ALK4 haplodeficiency on ventricular remodeling post-AAC. Consistent with our previous study,[18] AAC-induced upregulation of ALK4 protein expression in LV was significantly alleviated in $ALK4^{+/-}$ ventricles (Figure S2A). Heart weight and the size of ventricular myocyte were similar between $ALK4^{+/-}$ mice and WT littermates post-AAC (Figure S2B, S2D, S2F). However, $ALK4^{+/-}$ mice showed a significantly ameliorated ventricular interstitial fibrosis in comparison with WT littermates post-AAC (Figure S2D and S2E). Compared with WT littermates, LV gene expression associated with hypertrophy, including atrial natriuretic peptide, brain natriuretic peptide, and β-myosin heavy chain was also significantly downregulated in $ALK4^{+/-}$ mice post-AAC (Figure S2C). Moreover, ALK4 haplodeficiency ameliorated AAC-induced cardiac dysfunction, as reflected by improvement in ejection fraction and lung weight (Figure S3A through S3C).

ALK4 Haplodeficiency Protects Against AAC-Induced Atrial Fibrosis but Not Atrial Hypertrophy and Dilatation

Similar to changes observed in LV, ALK4 expression was gradually upregulated in the LA over 4 to 8 weeks post-AAC, and AAC-induced upregulation of ALK4 protein expression in LA was significantly alleviated in atria of $ALK4^{+/-}$ mice (Figure 1A). Moreover, LV end-diastolic pressure was increased in both WT littermates and $ALK4^{+/-}$ mice post-AAC compared with corresponding sham mice. However, LV end-diastolic pressure was significantly lower in $ALK4^{+/-}$ mice compared with WT littermates after 4 or 8 weeks post-AAC (Figure 1B). In the atria, AAC caused similar trends of increased cellular diameter and weight of combined atria in both $ALK4^{+/-}$ mice and WT littermates at 4 or 8 weeks post-AAC (Figure 1C through 1E). AAC-induced enhanced expressions of atrial hypertrophy–associated genes including brain natriuretic peptide and growth differentiation factor 15 in pooled atria were significantly lower in $ALK4^{+/-}$ mice than in WT littermates at 8 weeks post-AAC. However, atrial natriuretic peptide expression was not significantly increased in either genotype (Figure 1G). LA length measured by echocardiography tended to increase in response to AAC, but this did not reach statistical significance in either genotype (Figure 1F).

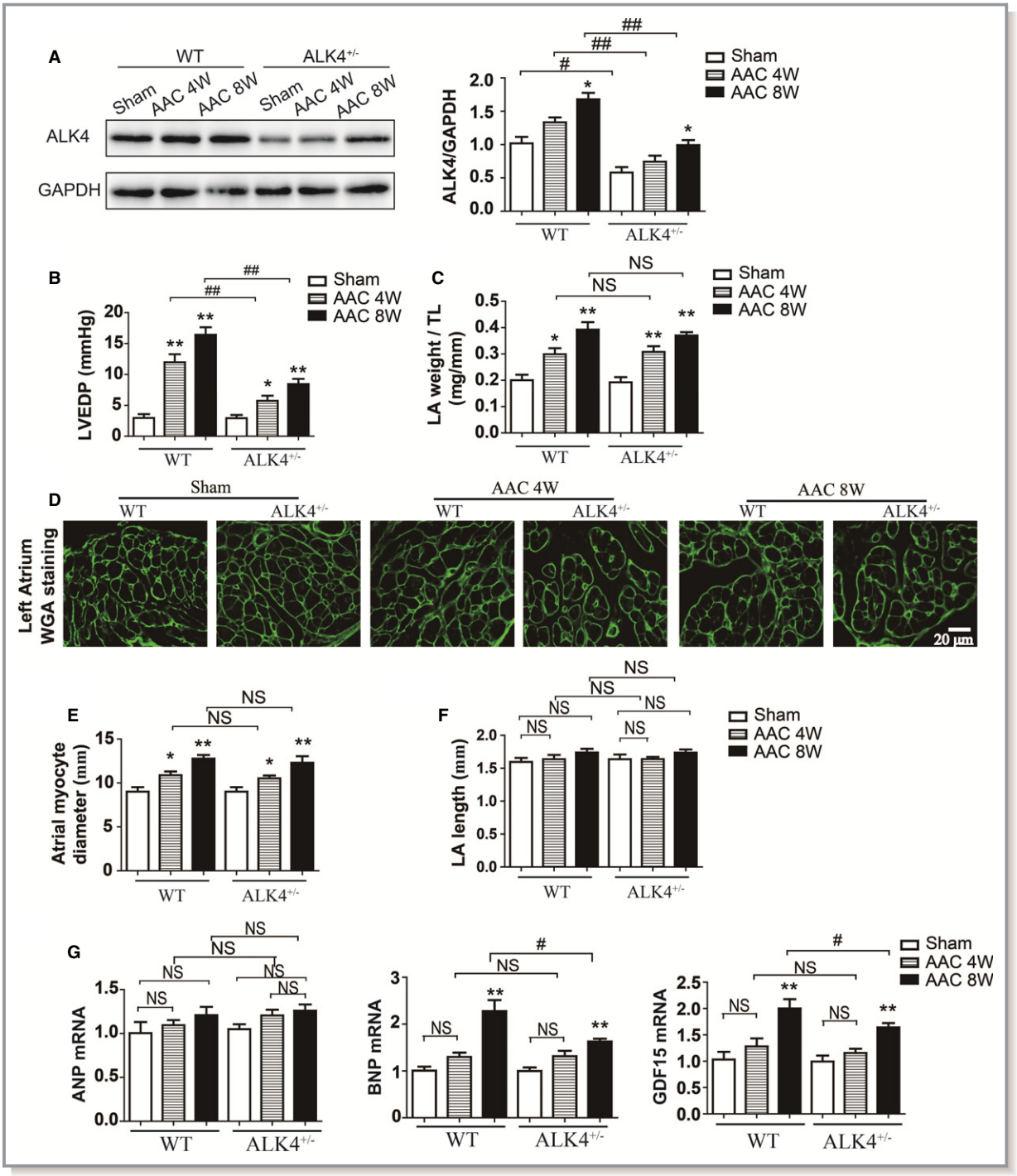

Figure 1. The effects of ventricular pressure on AAC-induced atrial hypertrophy and atrial dilatation in ALK4$^{+/-}$ mice and WT littermates. A, Changes in ALK4 protein expression by Western blotting in the left atria of ALK4$^{+/-}$ mice and WT littermates at 4 or 8 weeks post-AAC (n=5 in each group). B, LVEDP and (C) the left atrium weight-to–tibia length ratio (LA weight/TL) were compared between the 2 genotypes at 4 or 8 weeks post-AAC (n=8 in each group). D, Representative images of WGA staining of the left atrium tissues obtained at 4 or 8 weeks post-AAC in ALK4$^{+/-}$ mice and WT littermates. The scale bar is 20 μm. E, Quantification of the left atrium myocyte cross-sectional area based on WGA staining (n=6 in each group, ≥100 cells per group) in ALK4$^{+/-}$ mice and WT littermates between sham and AAC groups. F, Left atrium length measured by echocardiography in indicated groups (n=8 in each group). G, mRNA expression of ANP, BNP, and GDF15 of left atria from ALK4$^{+/-}$ mice and WT littermates after sham surgery or AAC (n=4 in each group). Data are presented as mean±SEM. *P<0.05, **P<0.01 vs corresponding sham group. $^{\#}P$<0.05, $^{\#\#}P$<0.01 vs corresponding WT group. AAC indicates abdominal aortic constriction; ALK4, Activin receptor-like kinase 4; ANP, atrial natriuretic peptide; BNP, brain natriuretic peptide; GDF15, growth differentiation factor 15; LA, left atrium; LVEDP, left ventricle end-diastolic pressure; NS, not significant; TL, tibia length; 4W, 4 weeks postprocedure; 8W, 8 weeks postprocedure; WGA, wheat germ agglutinin; WT, wild type.

In pooled atria, picrosirius red staining showed similarly increased fibrosis in both ALK4$^{+/-}$ mice and WT littermates at 4 weeks post-AAC. However, aggravation of atrial interstitial fibrosis was significantly reduced in ALK4$^{+/-}$ mice compared with WT littermates at 8 weeks post-AAC (Figure 2A and 2B). Meanwhile, atrial expression of collagen I was significantly increased at 8 weeks post-AAC in WT littermates, which was significantly downregulated in ALK4$^{+/-}$ mice after 8 weeks from ACC (Figure 2C). Because there were more obvious differences in atrial fibrosis– and atrial hypertrophy–associated gene expression between ALK4$^{+/-}$ mice and WT littermates at 8 weeks post-AAC, we only use the 8-week AAC model in the following study to explore the effects of ALK4 haplodeficiency on pressure overload–induced atrial remodeling.

As shown in Figure 2D, AAC induced more elevated expression of α-SMA, and proliferation cellular nuclear antigen in atria of WT littermates than in atria of ALK4$^{+/-}$ mice. As is well known, α-SMA is a marker of the fibroblast transformation to a myofibroblast. However, α-SMA could gradually be reexpressed in atrial myocytes during persistent atrial fibrillation,[30] and this seems to be confirmed by the α-SMA staining in the AAC model at 8 weeks shown in Figure 2E. So the α-SMA staining partly represents the myofibroblasts. Because the cardiomyocyte could hardly proliferate, we further evaluated myofibroblast proliferation by costaining Ki67 and α-SMA. The number of Ki67-positive myofibroblasts was significantly higher in LA sections of WT littermates than in those of ALK4$^{+/-}$ mice post-AAC (Figure 2E), hinting that ALK4 haplodeficiency blocked the proliferation of myofibroblasts in atria. Meanwhile, CCK-8 assays showed that the proliferation of atrial fibroblasts extracted from the ALK4$^{+/-}$ mice post-AAC was slower than that of those extracted from the WT littermates post-AAC (Figure 3A), and ALK4 haplodeficiency blocked AAC-induced upregulation of α-SMA and connective tissue growth factor expression. All these results revealed that haplodeficient ALK4 blocked proliferation, differentiation, and extracellular matrix synthesis capacity of atrial fibroblasts (Figure 3B).

ALK4 Haplodeficiency Protects Against AAC-Induced Alterations of Gap Junction Proteins in Atria

In atria, Cx40 and Cx43 present the major cardiac gap junctions. Western blotting showed reduced Cx40 protein level and Cx40/Cx43 ratio as well as increased Cx43 protein level post-AAC in the atrial samples of WT littermates, which were not shown in ALK4$^{+/-}$ mice (Figure 4A and 4B). We also studied the distribution of Cx40 and Cx43 in the atria of ALK4$^{+/-}$ mice and WT littermates. As shown in Figure 4C, Cx40 could be detected in discrete spots post-AAC (presumably corresponding to gap junction plaques). However, AAC-induced upregulation of Cx43 proteins in WT littermates was more prone to redistribute to the lateral membranes as compared with ALK4$^{+/-}$ mice (Figure 4D). These results indicated that reduction of functional Cx40 in atrial gap junctions and increase of Cx43 lateral redistribution might contribute to the AAC-induced electrical remodeling, thus facilitating the progression of AF.

ALK4 Haplodeficiency Protects Against AAC-Induced Inflammation in Atria

Inflammation was evidenced by upregulated expression of interleukin-6 and monocyte chemotactic protein 1 in the atrial samples of both ALK4$^{+/-}$ mice and WT littermates at 8 weeks post-AAC. ALK4 haplodeficiency partially blocked AAC-induced upregulation of these inflammatory cytokines (Figure 5A and 5B). Meanwhile, in consideration of evident macrophage infiltration in atria of the AAC model, we performed a transwell assay to explore the chemotaxis of macrophages in each group. As shown in Figure 5C, atrial fibroblasts extracted from WT littermates post-AAC induced obvious chemotaxis of macrophages extracted from WT littermates post-AAC. However, atrial fibroblasts extracted from ALK4$^{+/-}$ mice post-AAC blocked chemotaxis of macrophages extracted from ALK4$^{+/-}$ mice post-AAC. Taken together, these findings collectively suggested that ALK4 haplodeficiency protected against AAC-induced inflammation in atria, especially the chemotaxis of macrophages.

ALK4 Haplodeficiency Inhibited AAC-Induced Decreasd I_{Na}, $I_{Ca\text{-}L}$, and I_{K1} Current Densities and the Accompanying APD Shortening in Atrial Myocytes

Large numbers of studies have demonstrated that electrical remodeling was related to the pathogenesis of AF and resulted in alteration of APD or conduction velocity. We thus examined the expressions of ion channels contributing to the excitation of atrial myocytes. There were no major changes in expressions of KCND3, KCNQ1, KCNJ3, and KCNJ12 mRNA, which respectively encoded Kv4.3, Kv7.1, Kir3.1, and Kir2.2 separately and contributed to the cardiac transient outward potassium current (I_{to}), slow delayed rectifying potassium current (I_{Ks}), acetylcholine-activated inward rectifier K^+ current (I_{KAch}), and inward rectifier current (I_{K1}) (Figure 6A). However, expressions of CACNA1C, SCN5A, KCND2, and KCNJ2 mRNA were significantly downregulated in atrial samples from WT littermates subjected to AAC for 8 weeks, but these changes were not seen in atrial samples of ALK4$^{+/-}$ mice post-AAC

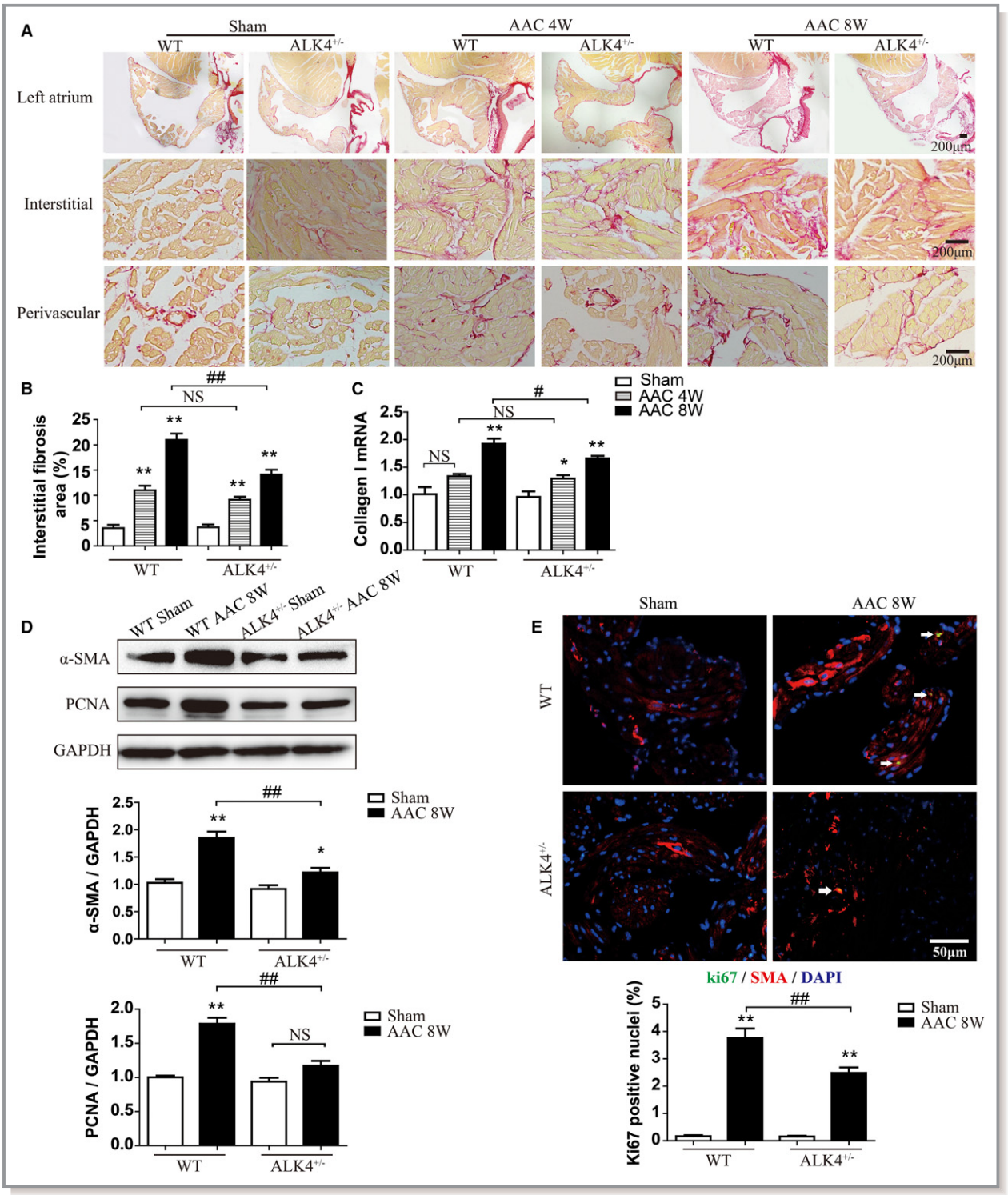

Figure 2. Haplodeficient ALK4 mitigated AAC-induced atrial fibrosis. A, Representative results of picrosirius red staining of the left atrium sections obtained from WT littermates and ALK4$^{+/-}$ mice at 4 or 8 weeks post-AAC (n=6 in each group; scale bar, 200 μm for all panels), and (B) statistical results of interstitial fibrosis area in left atrium (n=6 in each group; ≥40 fields per group). C, Relative mRNA level of collagen I in left atria obtained from ALK4$^{+/-}$ mice and WT littermates post-AAC (n=5 in each group). D, Changes in α-SMA and PCNA protein expression by Western blotting in the left atria of mice that underwent sham surgery or AAC in indicated groups (n=4 in each group). E, Representative images and quantitative results of staining Ki67 (green), α-SMA (red), and DAPI (blue) in left atrium sections of the indicated groups (n=6 in each group, ≥20 fields per group. Scale bar 50 μm). Data are presented as mean±SEM. *P<0.05, **P<0.01 vs corresponding sham group. $^{\#}P$<0.05, $^{\#\#}P$<0.01 vs corresponding WT group. AAC indicates abdominal aortic constriction; ALK4, Activin receptor-like kinase 4; NS, not significant; PCNA, proliferation cellular nuclear antigen; α-SMA, α-smooth muscle actin; 4W, 4 weeks postprocedure; 8W, 8 weeks postprocedure; WT, wild type.

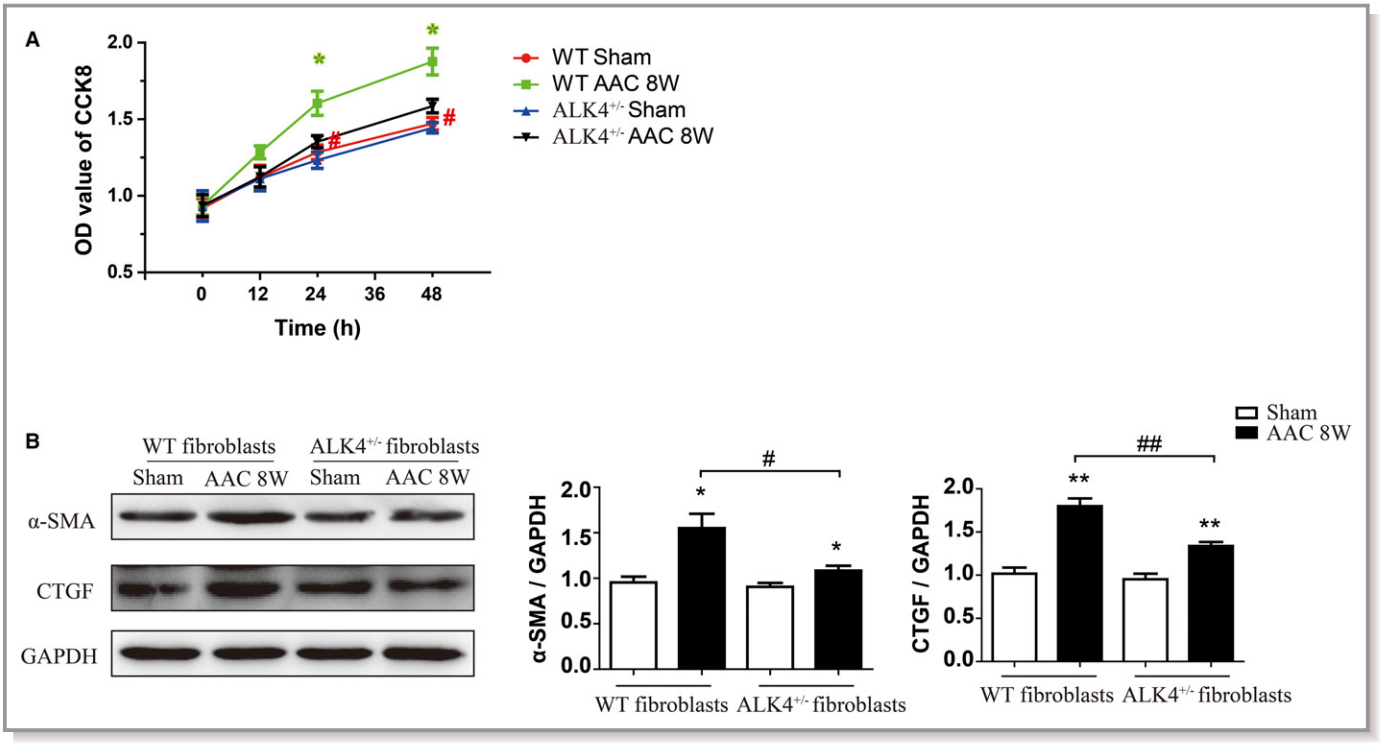

Figure 3. ALK4 haplodeficiency blocked AAC-induced proliferation, differentiation, and extracellular matrix synthesis capacity of atrial fibroblasts. A, CCK-8 assay (Dojindo olecular Technologies, Rockville, MD) of atrial fibroblast extracted from the ALK4$^{+/-}$ mice post-AAC, WT littermates post-AAC, and their corresponding sham group at 0, 12, 24, and 48 hours (n=5 in each group). B, Changes in α-SMA and CTGF protein expression by Western blotting in the atrial fibroblasts extracted from mice that underwent sham operations or AAC in indicated groups (n=4 in each group). Data are presented as mean±SEM. *P<0.05, **P<0.01 vs corresponding sham group. $^{\#}P$<0.05, $^{\#\#}P$<0.01 vs corresponding WT group. AAC indicates abdominal aortic constriction; ALK4, Activin receptor-like kinase 4; α-SMA, α-smooth muscle actin; CTGF, connective tissue growth factor; NS, nonsignificant; 8W, 8 weeks postprocedure.

(Figure 6A). These genes separately encoded Cav1.2, Nav1.5, Kv4.2, and Kir4.2 and then modulated L-type calcium channel ($I_{Ca\text{-}L}$), I_{Na}, I_{to}, and I_{K1}. The expression of KCNA5, which encoded Kv1.5 and modulated the slow delayed rectifying potassium current (I_{Ks}), showed the similar downward trend in both genotypes (Figure 6A). Furthermore, Western blotting showed that there were significant reductions in the expressions of CACNA1C and SCN5A proteins in WT littermates post-AAC, which were reversed by ALK4 haplodeficiency (Figure 6B).

Cellular electrophysiological experiments conducted by voltage clamp showed that AAC caused similar increases of cell capacitance in atrial myocyte isolated from ALK4$^{+/-}$ mice and WT littermates. Consistent with the results of wheat germ agglutinin staining, this finding further validates that AAC caused similar trends of increased cellular diameter in both genotypes (Figure 7A). To evaluate the effects of ALK4 haplodeficiency on AAC-induced electric activity of atrial myocytes, the APs were recorded and quantified. Figure 7B showed the AP morphology of atrial myocytes in each group. APD_{50} was significantly decreased to 21.8±7.1 milliseconds, and APD_{90} was decreased to 55.6±9.4 milliseconds in atrial myocytes of WT littermates post-AAC. However, ALK4 haplodeficiency inhibited or mitigated AAC-induced shortening of APD_{50} and APD_{90} (Figure 7C). Because differences exist in expressions of KCND2, CACNA1C, SCN5A, and KCNJ2 mRNA between atrial samples from WT littermates post-AAC and their corresponding ALK4$^{+/-}$ mice, we characterized the I_{to}, $I_{Ca\text{-}L}$, I_{Na}, and I_{K1} current in isolated atrial myocytes using a whole-cell patch clamp. Collectively, AAC induced decreased I_{to} current at +50 mV test pulse in WT atrial myocytes. ALK4$^{+/-}$ atrial myocytes and those post-AAC exhibited no significant difference in repolarizing I_{to} (Figure 7D). Meanwhile, for both WT and ALK4$^{+/-}$ atrial myocytes, AAC induced reduction of I_{Na} current density at voltages ranging from −50 to −25 mV. However, ALK4 haplodeficiency mitigated the downward trend in I_{Na} peak current density (Figure 7E). In contrast to the sham group, AAC significantly decreased $I_{Ca\text{-}L}$ and I_{K1} current density from −30 to +40 mV and from −120 to −60 mV. However, to some extent ALK4 haplodeficiency suppressed AAC-induced reduction of $I_{Ca\text{-}L}$ and I_{K1} (Figure 7F and 7G). Taken together, ALK4 haplodeficiency selectively mitigated AAC-induced reduction of I_{Na}, $I_{Ca\text{-}L}$, and I_{K1} current densities.

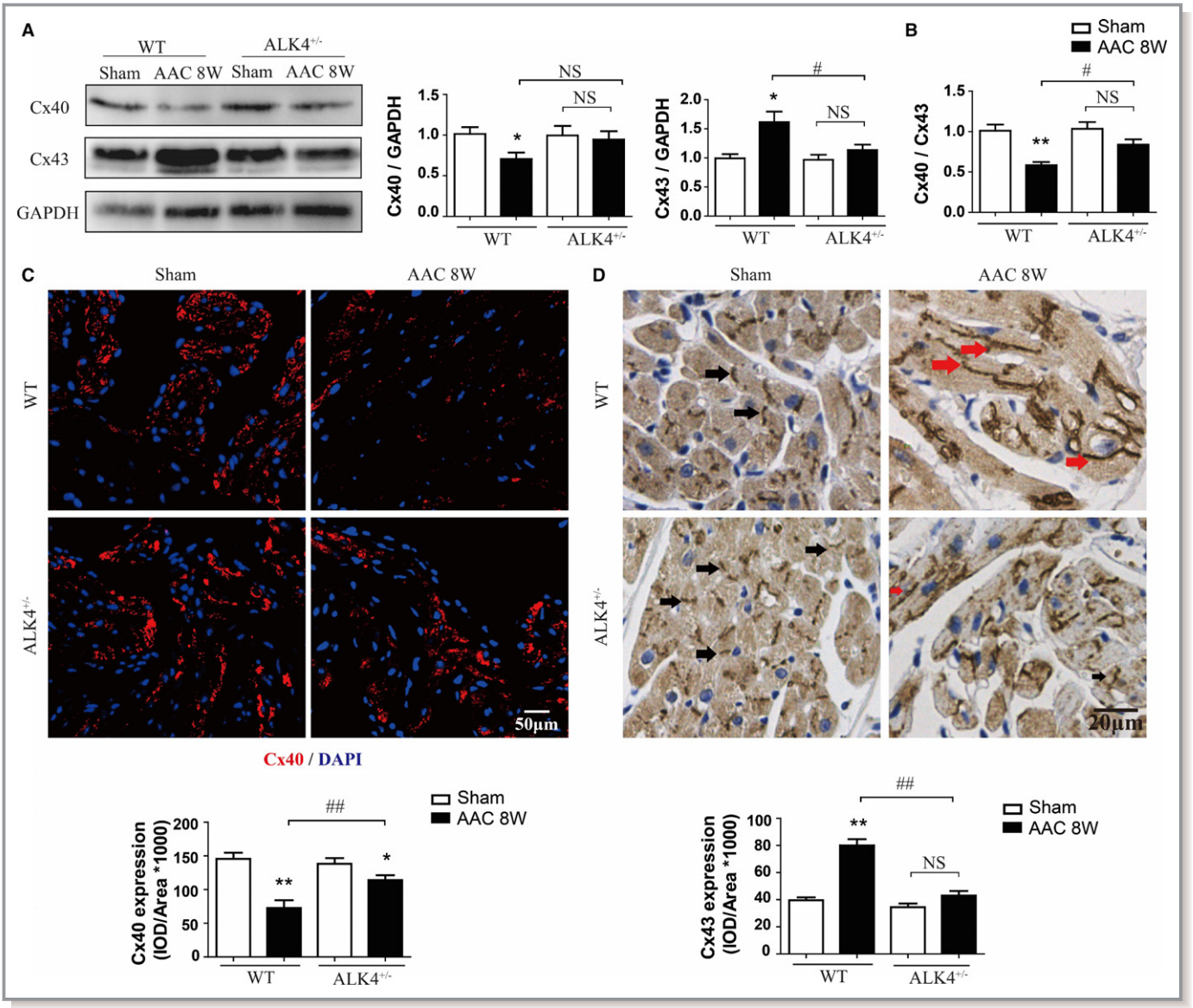

Figure 4. Haplodeficient ALK4 protected against AAC-induced alterations of gap junctions in atrium. A, Changes of Cx40, Cx43 expression and (B) the ratio of Cx40 expression to Cx43 expression in left atrium obtained from ALK4$^{+/-}$ mice and WT littermates at 8 weeks post-AAC by Western blotting (n=5 in each group). C, Representative immunofluorescence images and quantitative data on Cx40 expression in left atrium sections of the indicated groups (n=4 in each group, ≥10 fields per group. Scale bar 50 μm). D, Representative immunohistochemistry image and quantitative results of Cx43 staining in left atrium sections obtained from ALK4$^{+/-}$ mice and WT littermates at 8 weeks post-AAC. The black arrows indicate that Cx43 is localized in dense clusters at the ends of the cells, and the red arrows indicate that distribution of Cx43 markedly changes to the lateral side of the cells. (n=4 in each group. Scale bar 20 μm). Data are presented as mean±SEM. *P<0.05, **P<0.01 vs corresponding sham group. $^{\#}P$<0.05, $^{\#\#}P$<0.01 vs corresponding WT group. AAC indicates abdominal aortic constriction; ALK4, Activin receptor-like kinase 4; CTGF, connective tissue growth factor; Cx40, connexin 40; Cx43, connexin 43; NS, not significant; 8W, 8 weeks postprocedure; WT, wild type.

Electrophysiological Properties and AF Inducibility

To assess cardiac electrophysiological property in 2 genotypes, a surface ECG was recorded at 8 weeks post-AAC. Pressure overload for 8 weeks did not significantly affect heart rates of ALK4$^{+/-}$ mice or WT littermates (Figure 8A). In addition, interatrial conduction time based on P-wave duration showed a similar rising trend in both genotypes post-AAC (Figure 8B). Eight weeks after sham or AAC operation, a 1.1F catheter was inserted into the right atrium through the right jugular vein to evaluate the inducibility of AF in mice. Figure 8C shows representative AF induced by programmed atrial stimulation. There was less induction of AF in sham-operated WT littermates and ALK4$^{+/-}$ mice. AF was induced in 12 out of 15 (80.0%) WT littermates subjected to AAC for 8 weeks but in only 5 out of 15 (33.3%) ALK4$^{+/-}$ mice subjected to AAC for 8 weeks (Figure 8E). Similarly, WT

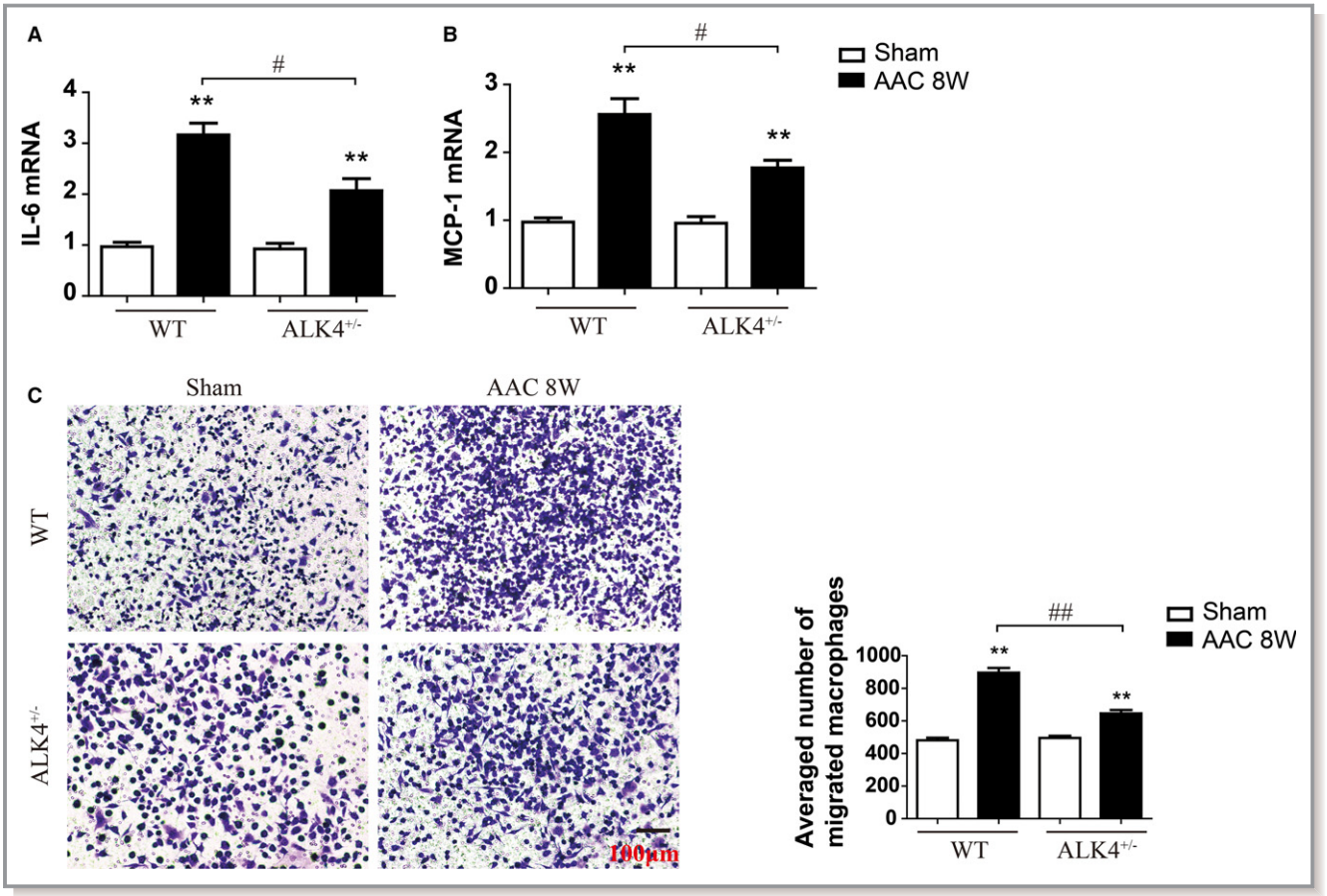

Figure 5. ALK4 haplodeficiency protected against AAC-induced inflammation in atria. A and B, Relative mRNA level of IL-6 and MCP-1 in left atria obtained from ALK4$^{+/-}$ mice and WT littermates post-AAC (n=4 in each group). C, Transwell assays were performed to determine AAC-induced chemotaxis of macrophages in each group. Atrial fibroblasts extracted from WT littermates post-AAC induced obvious chemotaxis of macrophages extracted from WT littermates post-AAC. However, atrial fibroblasts extracted from ALK4$^{+/-}$ mice post-AAC significantly blocked chemotaxis of macrophages extracted from ALK4$^{+/-}$ mice post-AAC (n=4 in each group. Scale bar 100 μm). Data are presented as mean±SEM. *P<0.05, **P<0.01 vs corresponding sham group. $^{\#}P$<0.05, $^{\#\#}P$<0.01 vs corresponding WT group. AAC indicates abdominal aortic constriction; ALK4, Activin receptor-like kinase 4; Cx40, connexin 40; Cx43, connexin 43; IL-6, interleukin-6; MCP-1, monocyte chemotactic protein 1; NS, not significant; 8W, 8 weeks postprocedure; WT, wild type.

littermates subjected to AAC for 8 weeks showed significantly increased AF duration compared with ALK4$^{+/-}$ mice exposed to AAC for 8 weeks (Figure 8F). Thus, ALK4 haplodeficiency preserved a significant protective effect against induction of AF in hypertrophied hearts.

ALK4 Haplodeficiency Attenuates Activation of the Smad2/3 Pathway

To elucidate the potential molecular mechanism regarding the function of ALK4 during AAC-induced atrial remodeling, we explored the well-known Smads and mitogen-activated protein kinase (MAPK) pathways in atrial samples of 4 groups. Consistent with our previous findings in LV, compared with WT littermates, ALK4$^{+/-}$ mice significantly blunted AAC-induced increases of phosphorylation of Smad2 and Smad3 in atrium at 8 weeks post-AAC (Figure 9A and 9B). The ratio of phosphorylated to total MAPKs, an indicator of phosphorylation-induced activation, was increased in atria of ALK4$^{+/-}$ mice and WT littermates at 8 weeks post-AAC, and the upward trend was almost the same (Figure 9A and 9C). These data suggested that ALK4 exerts beneficial effects on atrial remodeling post-AAC, possibly attributed to partial inactivation of the Smad2/3 pathway but not the MAPK pathway. Meanwhile, the effect of Smad3 inhibitor SIS3 was evaluated. Subcutaneous infusion of SIS3 by osmotic micropump induced less incidence of AF compared with those treated with vehicle alone during electrophysiological studies (Figure S4).

Impact of SB-431542 on AAC-Induced Atrial Remodeling

The effect of pharmacological blockade of ALK4 on AAC-induced atrial remodeling was assessed. Intraperitoneal administration with ALK4 inhibitor SB-431542 in WT

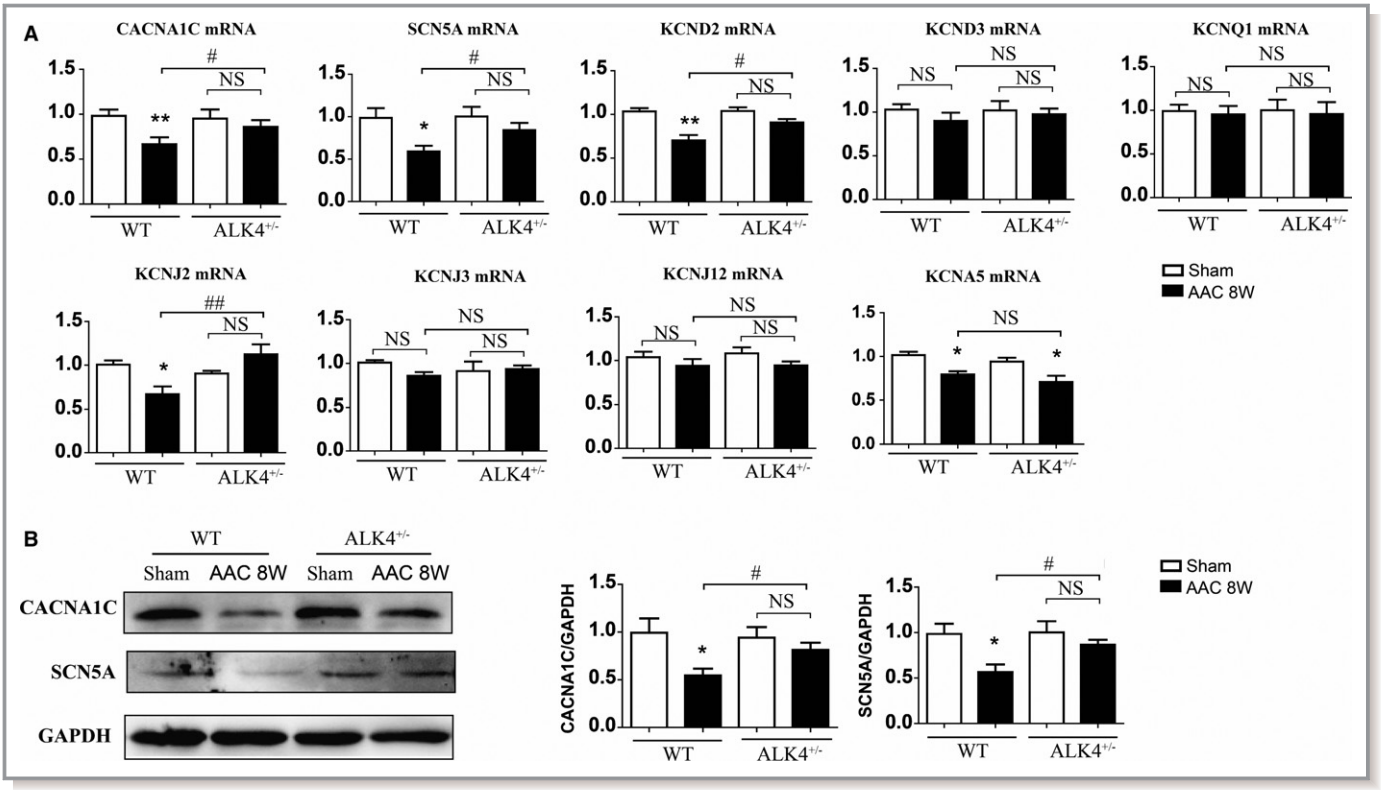

Figure 6. ALK4 haplodeficiency protects against AAC-induced electrical remodeling. A, Expression level of ion channels related to electrical remodeling in atrium. Relative mRNA level of CACNA1C, SCN5A, KCND2, KCND3, KCNQ1, KCNJ2, KCNJ3, KCNJ12, and KCNA5 in left atria obtained from ALK4$^{+/-}$ mice and WT littermates post-AAC (n=4 in each group). B, Changes of CACNA1C and SCN5A expression in left atria obtained from ALK4$^{+/-}$ mice and WT littermates at 8 weeks post-AAC by Western blotting (n=5 in each group). Data are presented as mean±SEM. *P<0.05, **P<0.01 vs corresponding sham group. $^{\#}P$<0.05, $^{\#\#}P$<0.01 vs corresponding WT group. AAC indicates abdominal aortic constriction; ALK4, Activin receptor-like kinase 4; CACNA1C, calcium voltage-gated channel subunit α1c; IL-6, interleukin-6; KCNA5, potassium voltage-gated channel, subfamily A, member 5; KCND2, potassium voltage-gated channel, Shal-related family, member 2; KCND3, potassium voltage-gated channel, Shal-related family, member 3; KCNJ12, potassium voltage-gated channel, subfamily J, member 12; KCNJ2, potassium voltage-gated channel, subfamily J, member 2; KCNJ3, potassium voltage-gated channel, subfamily J, member 3; KCNQ1, potassium voltage-gated channel, subfamily Q, member 1; MCP-1, monocyte chemotactic protein 1; NS, not significant; SCN5A, sodium voltage-gated channel α subunit 5; 8W, 8 weeks postprocedure; WT, wild type.

littermates resulted in reduced atrial interstitial fibrosis (Figure 10A and 10C), improved functional Cx40 expression (Figure 10B), and CACNA1C mRNA expression (Figure 10D) in atrium and less incidence of AF compared with those treated with vehicle alone during electrophysiological studies (Figure 10E through 10G). These results were consistent with the results obtained in ALK4$^{+/-}$ mice and suggested that administration of SB-431542 affected and finally partially attenuated AAC-induced atrial remodeling and thereby reduced the increased vulnerability of AF in mice subjected to AAC.

Discussion

In this study the potential protective effects of ALK4 haplodeficiency on atrial remodeling were examined in a chronic pressure-overload mouse model. Our results demonstrated that ALK4 haplodeficiency improved the arrhythmogenic substrate in atrium by reversing structural remodeling, electrophysiological remodeling, and inflammation, especially the chemotaxis of macrophages, and thus finally attenuated vulnerability to AF in a mouse model of AAC-induced hypertrophy through inactivation of the Smad2/3 pathway. These results suggest that a specific inhibitor of ALK4 will be a promising therapeutic target for the upstream prevention of AF in stressed hearts.

In our previous study a mouse model induced by continuous angiotensin II infusion was used to represent AF progression associated with fibrotic signals. The previous study only considered the effects of angiotensin II, a single factor, on the heart and only focused on atrial fibrosis not electrical remodeling and inflammation in the atrium. Most importantly, the previous study could not fully represent the pathophysiological process of most patients with AF in clinical

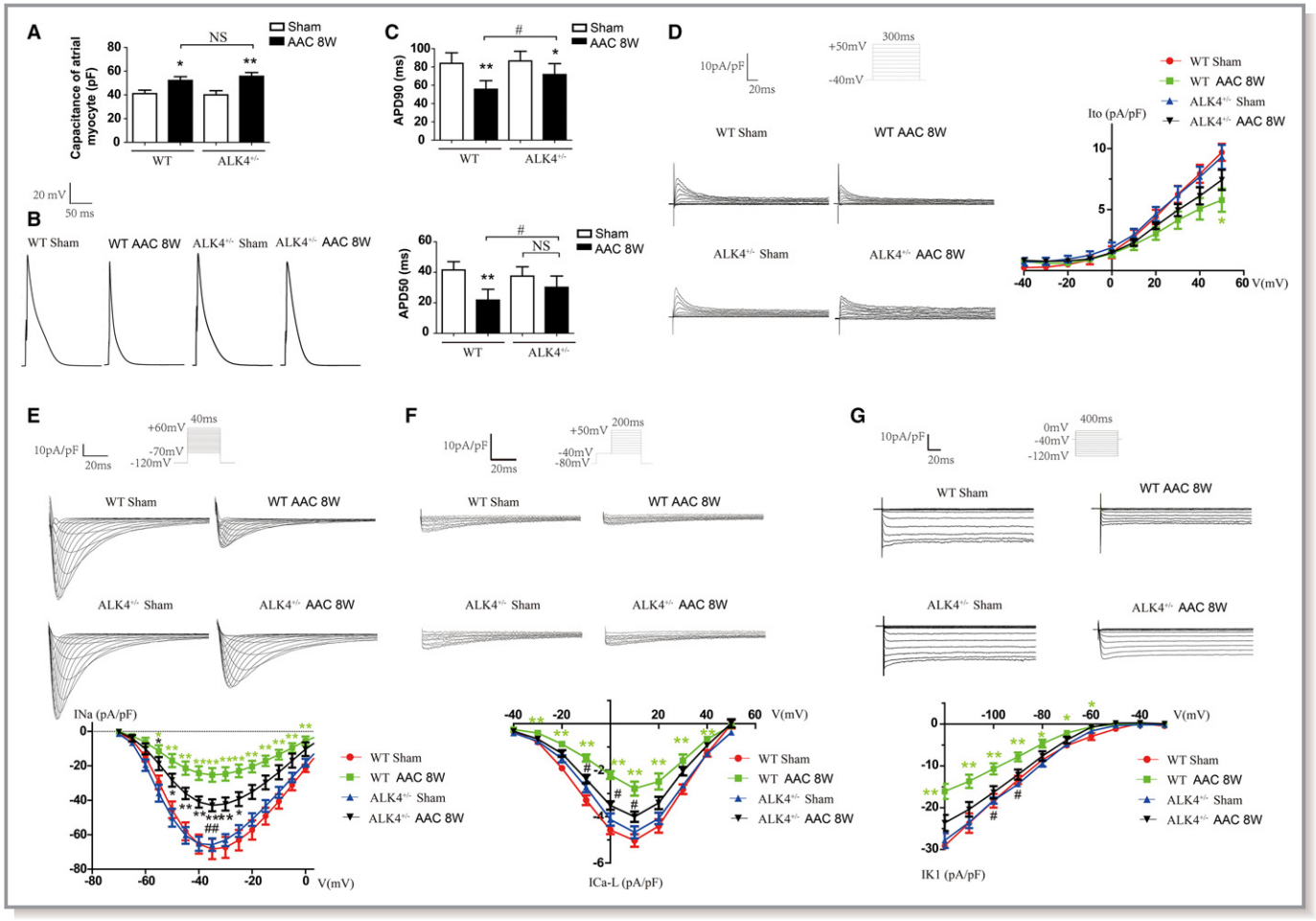

Figure 7. ALK4 haplodeficiency inhibited AAC-induced decreasd I_{Na}, $I_{Ca\text{-}L}$, I_{K1} current densities and the accompanying APD shortening in atrial myocytes. A, Whole-cell membrane capacitance of atrial myocytes isolated from ALK4$^{+/-}$ mice and WT littermates that underwent sham surgery or AAC (n=10 in each group). B, APs recorded from a representative atrial myocyte in each group at a pacing rate of 1 Hz. C, Averaged data of APD at 90% repolarization (APD_{90}) and APD at 50% repolarization (APD_{50}) under referred conditions. D, Representative original traces of whole-cell I_{to} current (300 ms depolarization step pulses from −40 to +50 mV with a step size of +10 mV) and representative density-voltage curve for I_{to} in atrial myocyte isolated from mice in each group. Insert, voltage protocol (n=8 in each group). E, Representative recordings of whole-cell I_{Na} current (sweep 1-sweep 16) in atrial myocyte isolated from mice in each group. Insert, voltage protocol. The lower panel shows representative I_{Na} density-voltage relationships in each group (n=8 in each group). F, Representative recordings of whole-cell $I_{Ca\text{-}L}$ current in atrial myocyte isolated from mice in each group. Insert, voltage protocol. The lower panel shows representative $I_{Ca\text{-}L}$ current density-voltage relationships in each group (n=8 in each group). G, Original representative recordings of the inwardly rectifier I_{K1} current (only voltage steps between −120 and −40 mV with a step size of +10 mV were shown) and representative density-voltage curve for I_{K1} in atrial myocyte isolated from mice in each group. Insert, voltage protocol. (n=8 in each group). Data were presented as mean±SEM. *P<0.05, **P<0.01 vs corresponding sham group. $^{\#}P$<0.05, $^{\#\#}P$<0.01 vs corresponding WT group. ALK4 indicates Activin receptor-like kinase 4; AP, action potential; NS, not significant; 8W, 8 weeks postprocedure.

practice. In this study a model of AAC was used to cause a sudden onset of pressure overload of the heart in ALK4$^{+/-}$ mice and WT littermates. This model is more representative of the LV hypertrophic processes observed in AF patients underlying hypertension. The AAC operation brings obvious alterations in ventricle, mainly including ventricular hypertrophy, apoptosis of ventricular myocytes, and proliferation and differentiation of fibroblasts. This operation also induces hemodynamic overload in atria and involves a series of alterations in the atria.[31] Liao et al demonstrated that 10 days of transverse aorta constriction induced increased atrial fibrosis and inflammation.[31] Other studies of pressure overload in mice also showed an increase in atrial diameter, atrial weight, atrial cellular hypertrophy, and increased AF inducibility.[1,5] As can be seen, this AAC model could best mimic the situation of newly developed AF in patients with hypertension due to the accompanied systemic inflammation, the increased LA wall stretch, and atrial interstitial fibrosis.[32]

Consistent with the findings in the ventricle, our study first demonstrated that although brain natriuretic peptide and growth differentiation factor 15 mRNA expressions were lower in atria of ALK4$^{+/-}$ mice than those in WT littermates

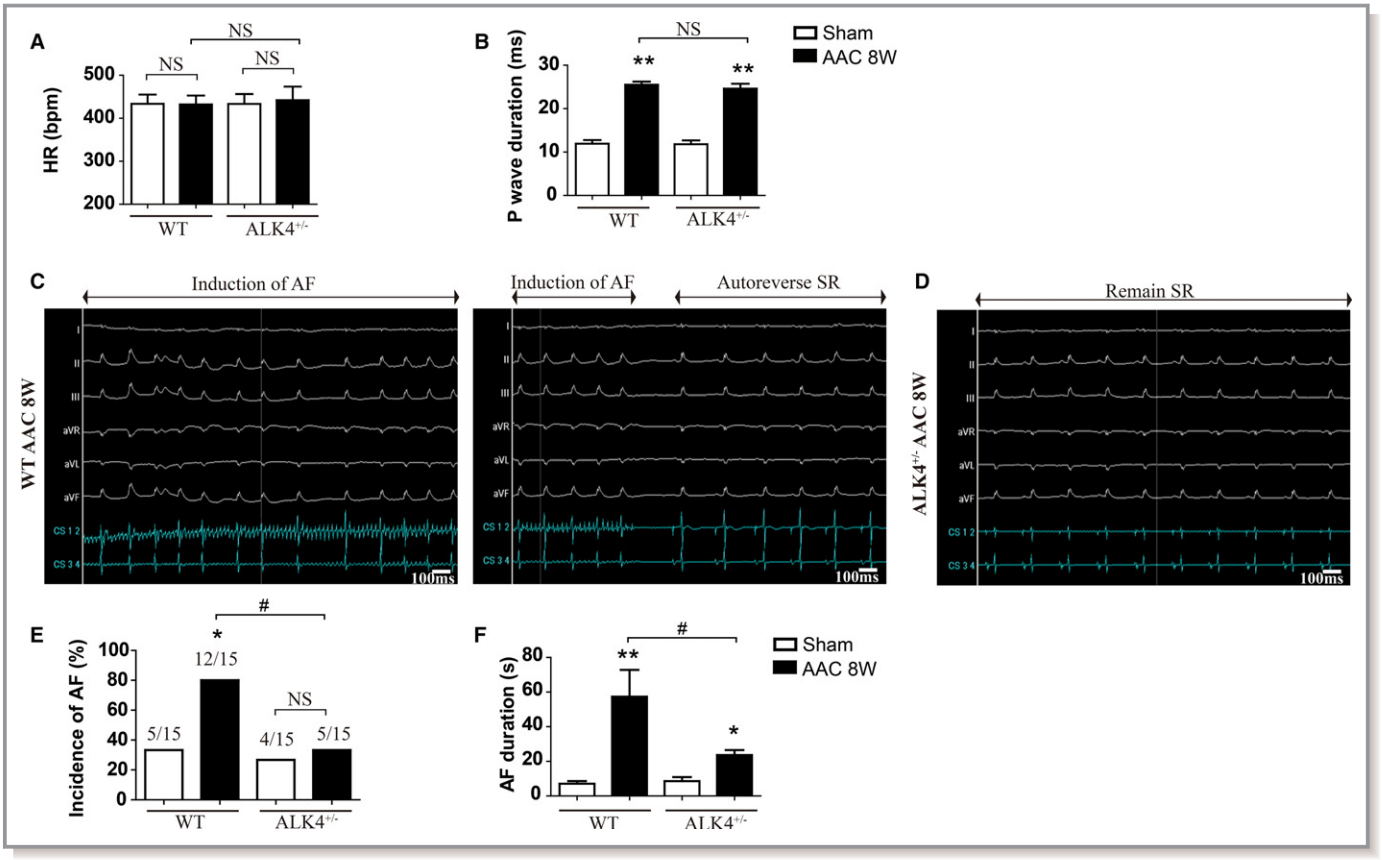

Figure 8. AF inducibility and duration in ALK4$^{+/-}$ mice and WT littermates subjected to sham or AAC operation. A, Heart rate and (B) P wave duration measured in vivo electrophysiological investigations using ALK4$^{+/-}$ mice and WT littermates after sham operation or AAC (n=6 in each group). C and D, Example electrical tracings of surface and intracardiac leads from (C) WT littermates and (D) ALK4$^{+/-}$ mice post-AAC during electrophysiological studies with cycle length of 40 milliseconds. Scale 100 milliseconds. E, Number and (F) total duration of AF episodes during the electrophysiological studies (n=15 in each group). Data are presented as mean±SEM. *P<0.05, **P<0.01 vs corresponding sham group. $^{\#}P$<0.05 vs corresponding WT group. AAC indicates abdominal aortic constriction; AF, atrial fibrillation; ALK4, Activin receptor-like kinase 4; HR, heart rate; NS, not significant; SR, sinus rhythm; 8W, 8 weeks postprocedure; WT, wild type.

after exposure to the AAC operation, ALK4 haplodeficiency did not affect the AAC-induced increase in the size of atrial myocytes and the ratio of LA weight and tibia length, which were the parameters of LA hypertrophy. These might be explained by the investigation described by Jeong et al that cardiac myocyte hypertrophy can be disassociated from expression of the pathological myocyte gene program.[33] So we speculate that AAC-induced increased ALK4 expression level in LA may be irrelevant to the synthesis of atrial hypertrophy–oriented proteins in the pressure-overloaded condition. Along with this, we observed an increasing trend toward atrial dilatation in both genotypes in response to increased ventricular pressure, but there was no statistical significance between them. This trend is possibly due to the smaller sample size of our study. Meanwhile, as an important contributor to the AF substrate, atrial fibrosis is the hallmark of atrial structural remodeling. The fibrous tissues physically separate atrial muscle fibers, thereby interrupting fiber bundle continuity and creating a physical barrier to conduction, which finally causes local conduction abnormalities. Our study demonstrated that ALK4 haplodeficiency exerts a protective effect on AAC-induced atrial fibrosis due to its blocking of the proliferation, differentiation, and synthesis capacity of the extracellular matrix of the atrial fibroblasts. Accordingly, this could partially inhibit local conduction abnormalities caused by AAC-induced atrial fibrosis. Furthermore, previous studies have revealed that inflammation contributes to the progression of AF.[34,35] The inflammatory response to pressure overload mediated by monocyte chemotactic protein 1, a key molecule in inflammatory fibrotic process, has been characterized in both ventricles and atria.[1] Our study showed that ALK4 haplodeficiency partially blocked AAC-induced upregulation of monocyte chemotactic protein 1. It is possible that ALK4 haplodeficiency attenuates atrial fibrosis partly via suppression of monocyte chemotactic protein 1 expression in atrium.

AF is associated with structural changes of the atrium, mainly including atrial dilation and increased interstitial

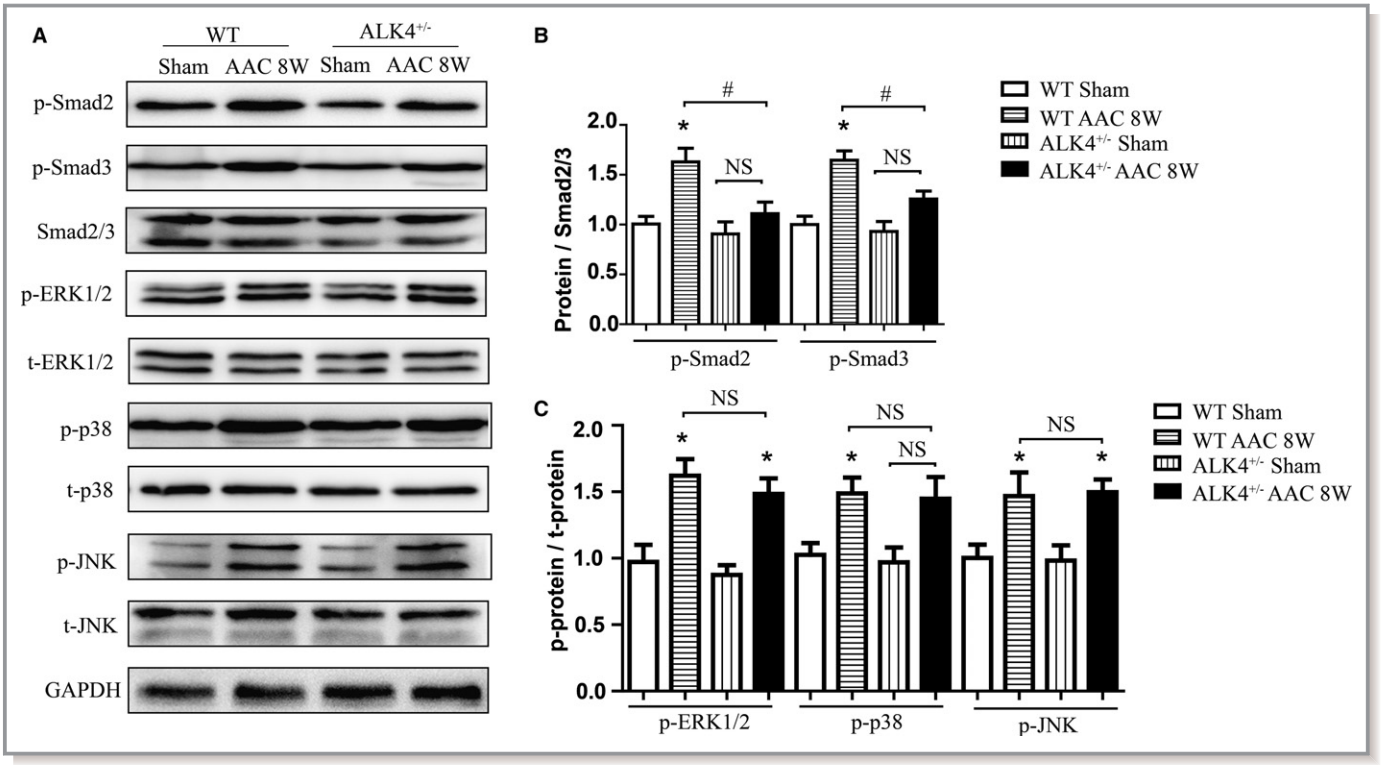

Figure 9. ALK4 haplodeficiency significantly blocks activation of Smad2/3 pathway in atrium. A, Representative Western blotting and quantitative data of (B) phosphorylation protein levels of Smad2, Smad3, (C) ERK, JNK and P38 of left atria from ALK4$^{+/-}$ mice and WT littermates after sham surgery or AAC (n=4 in each group). Data are presented as mean±SEM. *P<0.05 vs corresponding sham group. $^{\#}P$<0.05 vs corresponding WT group. AAC indicates abdominal aortic constriction; NS, not significant; ALK4, Activin receptor-like kinase 4; 8W, 8 weeks postsurgery; WT, wild type.

fibrosis as mentioned above. Meanwhile, AF of whatever cause leads to alterations in the electrophysiological properties of the atrial myocytes, and this is referred to as electrical remodeling. These 2 remodelings are involved in the perpetuation of AF.[36]

Atrial conduction depends on cell-to-cell communication, which is determined by gap junction channels. Cx40 and Cx43 are the primary components of the atrial gap junctions dominantly localized at the intercalated disk. Our understanding of the role of gap junctions in AF pathogenesis has increased enormously. Due to its central importance in cell-to-cell coupling, changes in expressions and distributions of connexin were widely studied in different cardiovascular diseases.[37] The vast majority of studies suggest that reduced abundance of Cx40 and heterogeneity of its distribution were common in atrial tissues from patients with AF.[38-40] There have been many conflicting results regarding the precise changes of Cx43 in AF.[39,41] At the animal level, transverse aortic constriction induced an increase in tyrosine phosphorylation of Cx43 in mice,[42] and downregulation of Cx43 expression was observed in LA and LV tissues of pressure-overloaded heart compared with that in the corresponding sham models.[37,42] Our study observed a reduced expression of Cx40 and Cx40/Cx43 ratio in the LA of WT littermates post-AAC, which conformed to the finding in patients with AF; however, there was a trend to higher expression of Cx43 in the AAC group. Of note, no evident changes related to AAC-induced gap junction remodeling were observed in ALK4$^{+/-}$ mice.

In regard to the expression of Cx43 in LA of WT littermates post-AAC, our finding is opposite to the finding of Shin et al.[37] Shin et al revealed that Cx43 mRNA expression in the LA was significantly decreased in the rats that underwent transverse aortic constriction. This discrepancy between our study and the previous study is possibly due to the following factors. First, a different situation of aortic constriction exists during the construction of the animal model. The aortic arch was constricted in most previous studies, whereas the abdominal aorta was constricted in our study. The extent of cardiac hypertrophy in these 2 models and the corresponding changes might be different. Second, Shin et al did not perform Western blot analysis because of the limitation in samples and thus could not clarify the expression of Cx43 protein. Finally, different durations of pressure overload exist in different studies, including 4, 8, or 12 weeks after operation. Here we conduct the 8-week AAC model in the

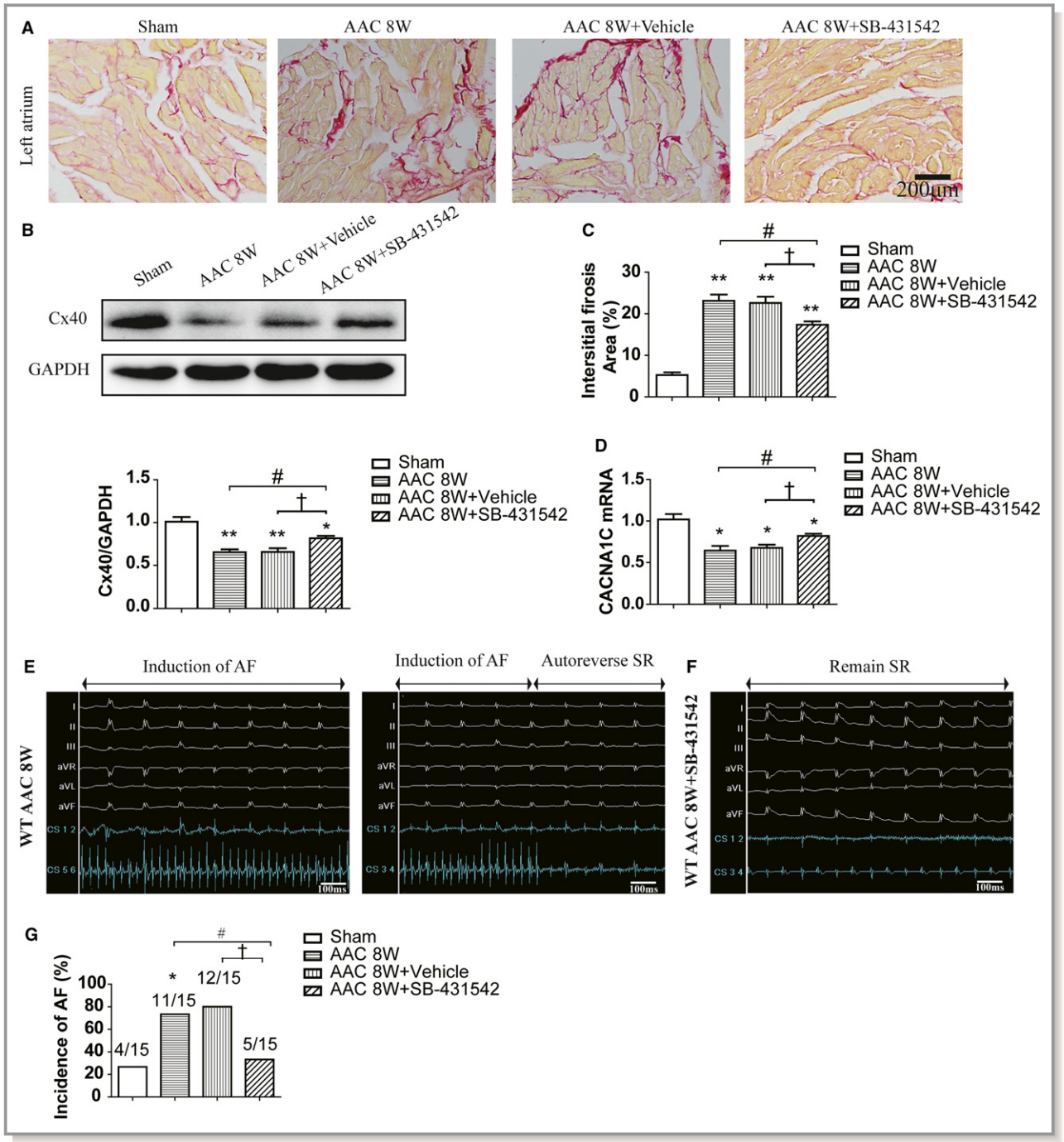

Figure 10. Intraperitoneal administration of ALK4 inhibitor SB-431542 inhibited atrial interstitial fibrosis, improved the expression of functional Cx40 protein and CACNA1C mRNA in atrium, and inhibited the vulnerability to AF at 8 weeks post-AAC. A, Representative results of picrosirius red staining of the left atrium sections obtained from WT littermates subjected to sham surgery or AAC or AAC operation with intraperitoneally administrated with SB-431542 (1 μmol/L solution, 100 μL/animal) or vehicle alone on first and third day and every 4 days after the production of AAC for 8 weeks (n=15 in each group; scale bar 200 μm). B, Representative western blots and quantitative data of Cx40 in left atrium obtained at 8 weeks post AAC in indicated groups (n=4 in each group). C, Statistical results of interstitial fibrosis area in left atrium (n=5 in each group). D, mRNA expression of CACNA1C in left atria from referred groups (n=4 in each group). E and F, Example electrical tracings of surface and intracardiac leads from (C) WT littermates post AAC and (D) WT littermates post AAC with intraperitoneal administrated with SB-431542 during electrophysiological studies with cycle length of 30 ms. Scale, 100 ms. G, Number of AF-episodes during the electrophysiological studies (n=15 in each group). Data are presented as mean±SEM. *P<0.05, **P<0.01 vs corresponding sham group. $^{\#}P$<0.05 vs corresponding AAC group. $^{\dagger}P$<0.05 vs corresponding AAC plus vehicle group. AAC indicates abdominal aortic constriction; ALK4, Activin receptor-like kinase 4; CACNA1C, calcium voltage-gated channel subunit α1c; Cx40, connexin 40; NS, not significant; SR, sinus rhythm; 8W, 8 weeks postsurgery; WT, wild type.

study. In order to further explain the discrepancy, we focused on the distribution of Cx43. We found that the AAC-induced upregulation of Cx43 proteins was more prone to redistribute to the lateral side of the cells. When the normal side-to-side gap junctions are redistributed at the lateral margins, the effective transverse propagation of conduction velocity decreases.[43] Together with a reduction in the amount of Cx40 and a specific reduced Cx40/Cx43 ratio, these results contributed to localized conduction abnormalities, thus facilitating the self-perpetuation of reentry pathways in AF.[40] However, ALK4 haplodeficiency blunted these changes and then played a protective role in the AAC-induced AF vulnerability.

Ion channel remodeling is the vital component of electrical remodeling that initially compensates, thereby maintaining cardiac performance, but over time it could become maladaptive, causing progressive heart failure and arrhythmias. Previous literature has indicated that there were varying degrees of changes in ionic channels concerning AF.[44] This may be explained by the fact that various models and species were used in experiments, such as animal models including rapid atrial pacing, angiotensin II stimulation, and aortic constriction or in vitro cultured atrial cardiomyocytes including mouse primary atrial myocytes, human primary atrial myocytes, and HL-1 cells. Our study used the model of AAC-induced AF and demonstrated that ALK4 haplodeficiency preserved AAC-induced decreased I_{Na} and $I_{Ca\text{-}L}$ density as well as the mRNA or protein expression of SCN5A and CACNA1C. As known, both currents were reported as affected by the pressure overload.[45,46] AAC-induced reductions in I_{Na} density, SCN5A gene expression and the accompanying decreased Cx40 expression potentially account for slowing of atrial conduction. Decreased conduction results in shorter wavelength and increases the number of wavelets that coexist in the atrial dimension, thus finally increasing the likelihood of sustained AF.[47] Thus, it is anticipated that the effects associated with the inhibition of AAC-induced decreased I_{Na} and Cx40 expression of ALK4 haplodificiency observed in this study might improve cardiac conduction. Meanwhile, AAC-induecd reduced $I_{Ca\text{-}L}$ decreased the I_{to} current, maintaining the plateau of the action potential, accelerating repolarization, shortening the AP duration, promoting reentry, and then facilitating the progression of AF.[48] The AAC itself induces the decrease of I_{to} current, which aggravates the changes mentioned above, further facilitating the induction and maintenance of reentry.[49] Haplodeficient ALK4 can effectively reverse $I_{Ca\text{-}L}$ density as well as the CACNA1C mRNA and protein expression post-AAC, blocking the calcium remodeling associated with AF. I_{k1} plays an important role in stabilizing the resting membrane potential and contributes to the late repolarization. ALK4 haplodeficiency also mitigated AAC-induced decreased I_{K1} current density. From this point of view, ALK4 haplodeficiency minimizes the downregulation of SCN5A and CACNA1C or functional impairment of I_{Na}, $I_{Ca\text{-}L}$, and I_{K1} induced by AAC and then produces beneficial effects against the adverse electrical remodeling in AAC-induced AF. Haplodeficient ALK4 finally partly blocks the AAC-induced electrical remodeling that leads to the progression of AF. Meanwhile, it is noted that changes of various currents contribute to the AAC-induced shortening of APD in atrial myocytes. APD shortening further promotes reentry and AF maintenance. ALK4 haplodeficiency significantly inhibits AAC-induced APD shortening and further prevents the induction and promotion of AF in an AAC model.

In all, as compared with WT littermates, $ALK4^{+/-}$ mice showed a remarkable reduction in the incidence and duration of AF episodes in hypertrophied hearts. The discrepancy in the incidence might be explained by the existence of discrepant histologically detectable atrial fibrosis, expressions of gap junction proteins, inflammation, and ion channels. All these changes correspond to the suppression of AF.

Mechanistically, as the downstream part of the ALK4, Smad2/3 pathway has been demonstrated to contribute to regulating the process of fibrosis[50] and the expression of connexin.[51,52] In the present study we observed an enhanced phosphorylation of Smad2 and Smad3 in atria of WT littermates post AAC. On the contrary, ALK4 haplodeficiency showed a significantly attenuated phosphorylation of Smad2 and Smad3 in LA tissues, suggesting that ALK4 prompted AAC-induced atrial remodeling by activating the Smad2/3 pathway. Meanwhile, because there is no agonist of Smad2 or Smad3, we could not observe whether activated Smad2 or Smad3 could abrogate the beneficial effects of ALK4 haplodeficiency. It is presumed that there is no specific inhibitor of Smad2, but SIS3, acting as a specific inhibitor of Smad3, could effectively inhibit Smad3 phosphorylation. Thus, in this study, we explore the effects of SIS3 on AAC-induced vulnerability to AF. Subcutaneous infusion of the Smad3 inhibitor SIS3 by osmotic micropump simulates the beneficial effects of ALK4 haplodeficiency on the inducibility of AF. This finding indirectly validates that the AAC-induced atrial remodeling, especially the electrophysiological remodeling, is possibly attributed to Smad3 activity. However, we could not rule out the equally important role of Smad2 activity in this process. In addition to the Smad2/3 pathway, ALK4 was also implicated in regulating MAPK pathways associated with cardiac remodeling and heart failure.[53] In our study we found that AAC induced similar upregulation of MAPK in the atria of both $ALK4^{+/-}$ mice and WT littermates. The above results demonstrate that, consistent with the finding in ventricles, ALK4 exerts a beneficial effect on atrial remodeling post-AAC mainly attributed to partial inactivation of the Smad2/3 pathway, not the MAPK pathway. Meanwhile, our studies concerning the use of pharmacologic inhibition of ALK4

in vitro highlighted that an ALK4 inhibitor could be a promising therapeutic target for the upstream prevention of AF in pressure-overloaded hearts. This comprehensive understanding of the protective role of haplodeficient ALK4 in the pathogenesis of AF in the stressed heart is expected to foster the development of improved pharmacological therapeutic approaches.

Conclusions

We demonstrated that ALK4 haplodeficiency ameliorated arrhythmogenic substrate in atrium by reversing structural remodeling, electrophysiological remodeling, and inflammation, especially the chemotaxis of macrophages, and thus finally attenuated vulnerability to AF in a mouse pressure-overload model associated with the suppression of Smad2/3 activity. These findings further suggest that ALK4 is a potential therapeutic target in treating pressure overload-induced AF.

Acknowledgments

We thank Dr Kai Hu from the Würzburg University in Germany for his help with the preparation of this manuscript.

Sources of Funding

This work was supported by the State Key Program of National Natural Science Foundation of China (No. 81530015 to Yi-Gang Li), National Natural Science Foundation of China grant (No. 81270258 to Yi-Gang Li, No. 81370257 and 81670414 to Yue-Peng Wang), Shanghai City Committee of Science and Technology Research Projects (No. 12411951900, 13140903801, and 14441902502 to Yi-Gang Li), and Doctoral Innovation Fund Projects from Shanghai Jiao Tong University School of Medicine (BXJ201723 to Qian Wang).

Disclosures

None.

References

1. Kume O, Takahashi N, Wakisaka O, Nagano-Torigoe Y, Teshima Y, Nakagawa M, Yufu K, Hara M, Saikawa T, Yoshimatsu H. Pioglitazone attenuates inflammatory atrial fibrosis and vulnerability to atrial fibrillation induced by pressure overload in rats. *Heart Rhythm*. 2011;8:278–285.
2. Dzeshka MS, Lip GY, Snezhitskiy V, Shantsila E. Cardiac fibrosis in patients with atrial fibrillation: mechanisms and clinical implications. *J Am Coll Cardiol*. 2015;66:943–959.
3. Nattel S, Dobrev D. Electrophysiological and molecular mechanisms of paroxysmal atrial fibrillation. *Nat Rev Cardiol*. 2016;13:575–590.
4. Lip GYH, Coca A, Kahan T, Boriani G, Manolis AS, Olsen MH, Oto A, Potpara TS, Steffel J, Marin F, de Oliveira Figueiredo MJ, de Simone G, Tzou WS, En Chiang C, Williams B. Hypertension and cardiac arrhythmias: executive summary of a consensus document from the European Heart Rhythm Association (EHRA) and ESC Council on Hypertension, endorsed by the Heart Rhythm Society (HRS), Asia-Pacific Heart Rhythm Society (APHRS), and Sociedad Latinoamericana de Estimulacion Cardiaca y Electrofisiologia (SOLEACE). *Eur Heart J Cardiovasc Pharmacother*. 2017;3:235–250.
5. De Jong AM, Van Gelder IC, Vreeswijk-Baudoin I, Cannon MV, Van Gilst WH, Maass AH. Atrial remodeling is directly related to end-diastolic left ventricular pressure in a mouse model of ventricular pressure overload. *PLoS One*. 2013;8:e72651.
6. Lau DH, Hendriks J, Kalman JM, Sanders P. Blood pressure control in atrial fibrillation: one of many critical components in risk factor modification. *Circulation*. 2017;135:1799–1801.
7. Miller JD, Aronis KN, Chrispin J, Patil KD, Marine JE, Martin SS, Blaha MJ, Blumenthal RS, Calkins H. Obesity, exercise, obstructive sleep apnea, and modifiable atherosclerotic cardiovascular disease risk factors in atrial fibrillation. *J Am Coll Cardiol*. 2015;66:2899–2906.
8. Wang Q, Yu Y, Zhang P, Chen Y, Li C, Chen J, Wang Y, Li Y. The crucial role of activin A/ALK4 pathway in the pathogenesis of Ang-II-induced atrial fibrosis and vulnerability to atrial fibrillation. *Basic Res Cardiol*. 2017;112:47.
9. Attisano L, Carcamo J, Ventura F, Weis FM, Massague J, Wrana JL. Identification of human activin and TGFβ type I receptors that form heteromeric kinase complexes with type II receptors. *Cell*. 1993;75:671–680.
10. Attisano L, Wrana JL, Montalvo E, Massague J. Activation of signalling by the activin receptor complex. *Mol Cell Biol*. 1996;16:1066–1073.
11. Heldin CH, Moustakas A. Signaling receptors for TGF-β family members. *Cold Spring Harb Perspect Biol*. 2016;8:a022053.
12. Gu Z, Nomura M, Simpson BB, Lei H, Feijen A, van den Eijnden-van Raaij J, Donahoe PK, Li E. The type I activin receptor ActRIB is required for egg cylinder organization and gastrulation in the mouse. *Genes Dev*. 1998;12:844–857.
13. Qiu W, Li X, Tang H, Huang AS, Panteleyev AA, Owens DM, Su GH. Conditional activin receptor type 1B (Acvr1B) knockout mice reveal hair loss abnormality. *J Invest Dermatol*. 2011;131:1067–1076.
14. Zheng J, Qu J, Lu P, Hou Z, Cui Y, Mao Y, Qi X, Ji H, Liu J. Activin A stimulates aromatase via the ALK4-Smad pathway in endometriosis. *Biomed Res Int*. 2016;2016:5791510.
15. Li Y, Klausen C, Zhu H, Leung PC. Activin A increases human trophoblast invasion by inducing SNAIL-mediated MMP2 up-regulation through ALK4. *J Clin Endocrinol Metab*. 2015;100:E1415–E1427.
16. Dean M, Davis DA, Burdette JE. Activin A stimulates migration of the fallopian tube epithelium, an origin of high-grade serous ovarian cancer, through non-canonical signaling. *Cancer Lett*. 2017;391:114–124.
17. Qiu W, Tang SM, Lee S, Turk AT, Sireci AN, Qiu A, Rose C, Xie C, Kitajewski J, Wen HJ, Crawford HC, Sims PA, Hruban RH, Remotti HE, Su GH. Loss of activin receptor type 1B accelerates development of intraductal papillary mucinous neoplasms in mice with activated KRAS. *Gastroenterology*. 2016;150:218–228.
18. Li CY, Chen YH, Wang Q, Hou JW, Wang H, Wang YP, Li YG. Partial inhibition of activin receptor-like kinase 4 attenuates pressure overload-induced cardiac fibrosis and improves cardiac function. *J Hypertens*. 2016;34:1766–1777.
19. Chen YH, Wang Q, Li CY, Hou JW, Chen XM, Zhou Q, Chen J, Wang YP, Li YG. Haplodeficiency of activin receptor-like kinase 4 alleviates myocardial infarction-induced cardiac fibrosis and preserves cardiac function. *J Mol Cell Cardiol*. 2017;105:1–11.
20. Li CY, Zhou Q, Yang LC, Chen YH, Hou JW, Guo K, Wang YP, Li YG. Dual-specificity phosphatase 14 protects the heart from aortic banding-induced cardiac hypertrophy and dysfunction through inactivation of TAK1-P38MAPK/-JNK1/2 signaling pathway. *Basic Res Cardiol*. 2016;111:19.
21. Tanaka H, Shinto O, Yashiro M, Yamazoe S, Iwauchi T, Muguruma K, Kubo N, Ohira M, Hirakawa K. Transforming growth factor β signaling inhibitor, SB-431542, induces maturation of dendritic cells and enhances anti-tumor activity. *Oncol Rep*. 2010;24:1637–1643.
22. Li J, Qu X, Yao J, Caruana G, Ricardo SD, Yamamoto Y, Yamamoto H, Bertram JF. Blockade of endothelial-mesenchymal transition by a Smad3 inhibitor delays the early development of streptozotocin-induced diabetic nephropathy. *Diabetes*. 2010;59:2612–2624.
23. Huang H, Tang Y, Wu G, Mei Y, Liu W, Liu X, Wan N, Liu Y, Huang C. ALK7 protects against pathological cardiac hypertrophy in mice. *Cardiovasc Res*. 2015;108:50–61.
24. Gu J, Liu X, Wang QX, Tan HW, Guo M, Jiang WF, Zhou L. Angiotensin II increases CTGF expression via MAPKs/TGF-β1/TRAF6 pathway in atrial fibroblasts. *Exp Cell Res*. 2012;318:2105–2115.
25. Pineda-Torra I, Gage M, de Juan A, Pello OM. Isolation, culture, and polarization of murine bone marrow-derived and peritoneal macrophages. *Methods Mol Biol*. 2015;1339:101–109.

26. Chen X, Bai Y, Sun H, Su Z, Guo J, Sun C, Du Z. Overexpression of M_3 muscarinic receptor suppressed adverse electrical remodeling in hypertrophic myocardium via increasing repolarizing K^+ currents. *Cell Physiol Biochem*. 2017;43:915–925.
27. Hou JW, Li W, Fei YD, Chen YH, Wang Q, Wang YP, Li YG. I_{CaL} and I_{to} mediate rate-dependent repolarization in rabbit atrial myocytes. *J Physiol Biochem*. 2018;74:57–67.
28. Hwang HR, Tai BY, Cheng PY, Chen PN, Sung PJ, Wen ZH, Hsu CH. Excavatolide B modulates the electrophysiological characteristics and calcium homeostasis of atrial myocytes. *Mar Drugs*. 2017;15:E25.
29. Zhang Y, Liu J, Liu Z, Wang M, Wang J, Lu S, Zhu L, Zeng X, Liang S. Effects of the venom of the spider *Ornithoctonus hainana* on neonatal rat ventricular myocytes cellular and ionic electrophysiology. *Toxicon*. 2014;87:104–112.
30. Ausma J, Litjens N, Lenders MH, Duimel H, Mast F, Wouters L, Ramaekers F, Allessie M, Borgers M. Time course of atrial fibrillation-induced cellular structural remodeling in atria of the goat. *J Mol Cell Cardiol*. 2001;33:2083–2094.
31. Liao CH, Akazawa H, Tamagawa M, Ito K, Yasuda N, Kudo Y, Yamamoto R, Ozasa Y, Fujimoto M, Wang P, Nakauchi H, Nakaya H, Komuro I. Cardiac mast cells cause atrial fibrillation through PDGF-A-mediated fibrosis in pressure-overloaded mouse hearts. *J Clin Invest*. 2010;120:242–253.
32. Hanif W, Alex L, Su Y, Shinde AV, Russo I, Li N, Frangogiannis NG. Left atrial remodeling, hypertrophy, and fibrosis in mouse models of heart failure. *Cardiovasc Pathol*. 2017;30:27–37.
33. Jeong MY, Kinugawa K, Vinson C, Long CS. AFos dissociates cardiac myocyte hypertrophy and expression of the pathological gene program. *Circulation*. 2005;111:1645–1651.
34. Hu YF, Chen YJ, Lin YJ, Chen SA. Inflammation and the pathogenesis of atrial fibrillation. *Nat Rev Cardiol*. 2015;12:230–243.
35. Harada M, Van Wagoner DR, Nattel S. Role of inflammation in atrial fibrillation pathophysiology and management. *Circ J*. 2015;79:495–502.
36. Gassanov N, Brandt MC, Michels G, Lindner M, Er F, Hoppe UC. Angiotensin II-induced changes of calcium sparks and ionic currents in human atrial myocytes: potential role for early remodeling in atrial fibrillation. *Cell Calcium*. 2006;39:175–186.
37. Shin SY, Jo WM, Min TJ, Kim BK, Song DH, Hyeon SH, Kwon JE, Lee WS, Lee KJ, Kim SW, Kim TH, Kim CJ, Im SI, Lim HE. Gap junction remodelling by chronic pressure overload is related to the increased susceptibility to atrial fibrillation in rat heart. *Europace*. 2015;17:655–663.
38. Gemel J, Levy AE, Simon AR, Bennett KB, Ai X, Akhter S, Beyer EC. Connexin40 abnormalities and atrial fibrillation in the human heart. *J Mol Cell Cardiol*. 2014;76:159–168.
39. Shu C, Huang W, Zeng Z, He Y, Luo B, Liu H, Li J, Xu J. Connexin 43 is involved in the sympathetic atrial fibrillation in canine and canine atrial myocytes. *Anatol J Cardiol*. 2017;18:3–9.
40. Wilhelm M, Kirste W, Kuly S, Amann K, Neuhuber W, Weyand M, Daniel WG, Garlichs C. Atrial distribution of connexin 40 and 43 in patients with intermittent, persistent, and postoperative atrial fibrillation. *Heart Lung Circ*. 2006;15:30–37.
41. Wetzel U, Boldt A, Lauschke J, Weigl J, Schirdewahn P, Dorszewski A, Doll N, Hindricks G, Dhein S, Kottkamp H. Expression of connexins 40 and 43 in human left atrium in atrial fibrillation of different aetiologies. *Heart*. 2005;91:166–170.
42. Yasuno S, Kuwahara K, Kinoshita H, Yamada C, Nakagawa Y, Usami S, Kuwabara Y, Ueshima K, Harada M, Nishikimi T, Nakao K. Angiotensin II type 1a receptor signalling directly contributes to the increased arrhythmogenicity in cardiac hypertrophy. *Br J Pharmacol*. 2013;170:1384–1395.
43. Polontchouk L, Haefliger JA, Ebelt B, Schaefer T, Stuhlmann D, Mehlhorn U, Kuhn-Regnier F, De Vivie ER, Dhein S. Effects of chronic atrial fibrillation on gap junction distribution in human and rat atria. *J Am Coll Cardiol*. 2001;38:883–891.
44. Gu J, Hu W, Liu X. Pioglitazone improves potassium channel remodeling induced by angiotensin II in atrial myocytes. *Med Sci Monit Basic Res*. 2014;20:153–160.
45. Kim JH, Jiang YP, Cohen IS, Lin RZ, Mathias RT. Pressure-overload-induced angiotensin-mediated early remodeling in mouse heart. *PLoS One*. 2017;12:e0176713.
46. Chen X, Qin M, Jiang W, Zhang Y, Liu X. Electrophysiological characteristics of pressure overload-induced cardiac hypertrophy and its influence on ventricular arrhythmias. *PLoS One*. 2017;12:e0183671.
47. Wang X, Li G. Irbesartan prevents sodium channel remodeling in a canine model of atrial fibrillation. *J Renin Angiotensin Aldosterone Syst*. 2018;19:1470320318755269.
48. Nattel S, Harada M. Atrial remodeling and atrial fibrillation: recent advances and translational perspectives. *J Am Coll Cardiol*. 2014;63:2335–2345.
49. Andrade J, Khairy P, Dobrev D, Nattel S. The clinical profile and pathophysiology of atrial fibrillation: relationships among clinical features, epidemiology, and mechanisms. *Circ Res*. 2014;114:1453–1468.
50. Zhang K, Han X, Zhang Z, Zheng L, Hu Z, Yao Q, Cui H, Shu G, Si M, Li C, Shi Z, Chen T, Han Y, Chang Y, Yao Z, Han T, Hong W. The liver-enriched lnc-LFAR1 promotes liver fibrosis by activating TGFβ and notch pathways. *Nat Commun*. 2017;8:144.
51. Hou J, Wang L, Hou J, Guo T, Xing Y, Zheng S, Zhou C, Huang H, Long H, Zhong T, Wu Q, Wang J, Wang T. Peroxisome proliferator-activated receptor gamma promotes mesenchymal stem cells to express connexin43 via the inhibition of TGF-β1/Smads signaling in a rat model of myocardial infarction. *Stem Cell Rev*. 2015;11:885–899.
52. Hou J, Yan P, Guo T, Xing Y, Zheng S, Zhou C, Huang H, Long H, Zhong T, Wu Q, Wang J, Wang T. Cardiac stem cells transplantation enhances the expression of connexin 43 via the ANG II/AT1R/TGF-beta1 signaling pathway in a rat model of myocardial infarction. *Exp Mol Pathol*. 2015;99:693–701.
53. Hu J, Wang X, Wei SM, Tang YH, Zhou Q, Huang CX. Activin A stimulates the proliferation and differentiation of cardiac fibroblasts via the ERK1/2 and p38-MAPK pathways. *Eur J Pharmacol*. 2016;789:319–327.

SUPPLEMENTAL MATERIAL

Table S1 Clinical Characteristics of Patients with AF or SR

	SR (n=10)	AF (n=10)		
		AF underlying hypertension (n=5)	AF devoid of hypertension (n=5)	AF (Total, n=10)
Age (years)	63.40±11.23	60.60±11.20	64.80±14.04	62.70±12.18
Male n (%)	3 (30.00%)	2 (40.00%)	2 (40.00%)	4 (40.00%)
Echocardiographic parameters				
LA diameter (cm)	4.06±0.51	4.48±0.34	4.39±0.37	4.44±0.34
LA volume (ml)	65.94±15.55	73.77±15.88	69.66±13.53	71.72±14.08
LVEF (%)	57.10±7.27	57.87±5.55	56.87±7.48	57.37±6.23
IVSd (mm)	9.20±2.25	12.20±2.05	9.00±2.00*	10.60±2.54

AF, atrial fibrillation; SR, sinus rhythm; LA, left atrium; LVEF, left ventricular ejection fraction; IVSd, diastolic interventricular septum.
*$p < 0.01$ vs AF underlying hypertension

Table S2 Tables of sequences for upstream and downstream primers for genes analyzed by real-time PCR

Gene	Forward Primer	Reverse Primer
GAPDH	5'-ACTCCACTCACGGCAAATTC-3'	5'-TCTCCATGGTGGTGAAGACA-3'
Collagen I	5'-AGGCTTCAGTGGTTTGGATG-3'	5'-CACCAACAGCACCATCGTTA-3'
ANP	5'-ACCTGCTAGACCACCTGGAG-3'	5'-CCTTGGCTGTTATCTTCGGTACCGG-3
BNP	5'-GAGGTCACTCCTATCCTCTGG-3'	5'-GCCATTTCCTCCGACTTTTCTC-3'
β-MHC	5'- CCGAGTCCCAGGTCAACAA-3'	5'- CTTCACGGGCACCCTTGGA-3'
GDF15	5'-CTGGCAATGCCTGAACAACG-3'	5'-GGTCGGGACTTGGTTCTGAG-3'
IL-6	5'-TAGTCCTTCCTACCCCAATTTCC-3'	5'-TTGGTCCTTAGCCACTCCTTC-3'
MCP-1	5'-GCCAACTCTCACTGAAGCC-3'	5'-GCTGGTGAATGAGTAGCAGC-3'
CACNA1C	5'-AGATCCAGCCATCTCCAAAGAG-3'	5'-CCTTTTGTCGCTTTAGACATTCC-3'
SCN5A	5'-ATGGCAAACTTCCTGTTACCTC-3'	5'-CCACGGGCTTGTTTTTCAGC-3'
KCND2	5'-TAGAGGCAGTGTGCAAGAAC-3'	5'-ATTGCTGTGGTCACGTAAGG-3'
KCND3	5'-ACACCTGCCCAACTCTAAC-3'	5'-CAGTCCATCGTCTGCTTTC-3'
KCNQ1	5'-GCAAAGACCGTGGCAGTAAC-3'	5'-ATGGACAGCAGCTGGTGGAG-3'
KCNJ2	5'-CGGCTCATTCTCTTTCAC-3'	5'-ATGGATGCTTCCGAGAAC-3'
KCNJ3	5'-CTGGAGGCATTGTGGAAAC-3'	5'-GCATGGAACTGGGAGTAATC-3'
KCNJ12	5'-ACCCCTACAGCATCGTATCAT-3'	5'-GTTGCACTGACCGTTCTTCTT-3'
KCNA5	5'-TCAAGGAAGAGGAGAAGCCC-3'	5'-GAATGACCAAGACCGACACG-3'

ANP, atrial natriuretic peptide; BNP, brain natriuretic peptide; β-MHC, β-myosin heavy chain; GDF15, growth differentiation factor 15; IL-6, interleukin-6; MCP-1, monocyte chemoattracion protein 1; CACNA1C, calcium voltage-gated channel subunit α1c; SCN5A, sodium voltage-gated channel alpha subunit 5, KCND2, potassium voltage-gated channel, Shal-related family, member 2; KCND3, potassium voltage-gated channel, Shal-related family, member 3; KCNQ1, potassium voltage-gated channel, subfamily Q, member 1; KCNJ2, potassium voltage-gated channel, subfamily J, member 2; KCNJ3, potassium voltage-gated channel, subfamily J, member 3; KCNJ12, potassium voltage-gated channel, subfamily J, member 12; KCNA5, potassium voltage-gated channel, subfamily A, member 5.

Figure S1

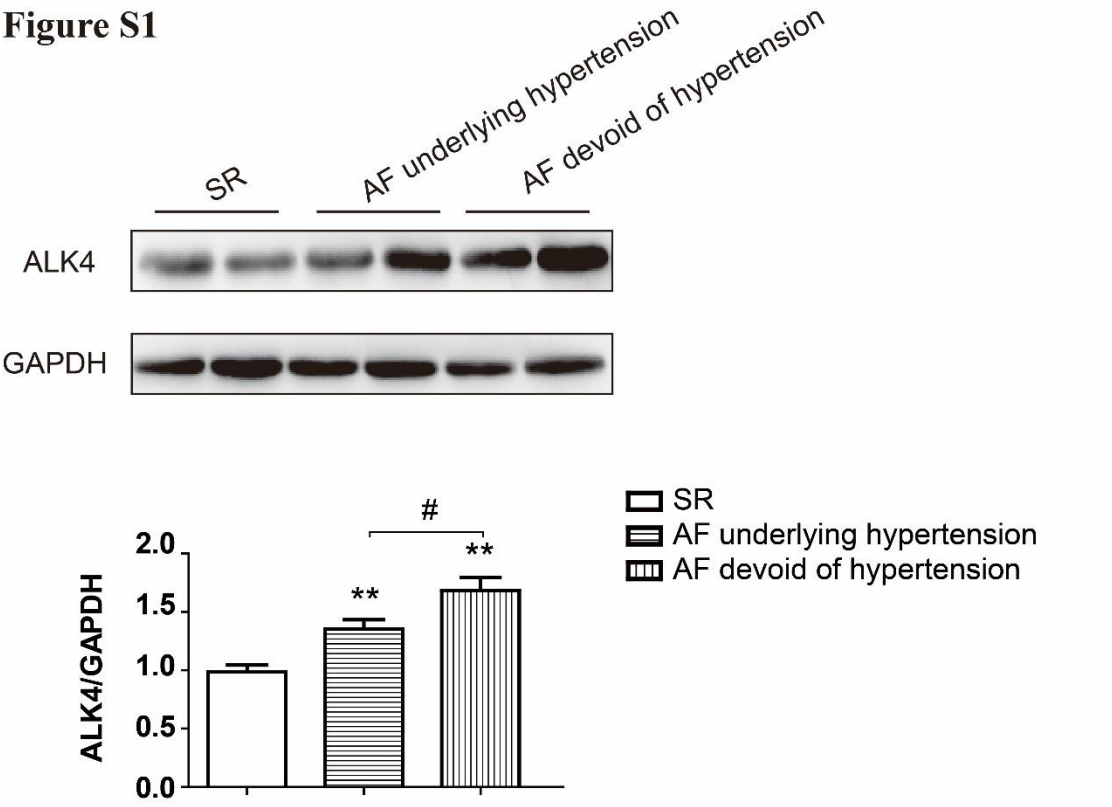

Figure S1. The protein expression of ALK4 is upregulated in the atria obtained from AF patients, and among them, AF patients underlying hypertension had higher ALK4 expression.

Western blotting analysis of ALK4 in the atria obtained from patients with SR, AF patients with hypertension and AF patients avoid of hypertension (n=5 in each group). $^{*}p < 0.05$, $^{**}p < 0.01$ vs corresponding SR group. $^{\#}p < 0.05$, $^{\#\#}p < 0.01$ vs AF patients with hypertension group. AF, atrial fibrillation; SR, sinus rhythm.

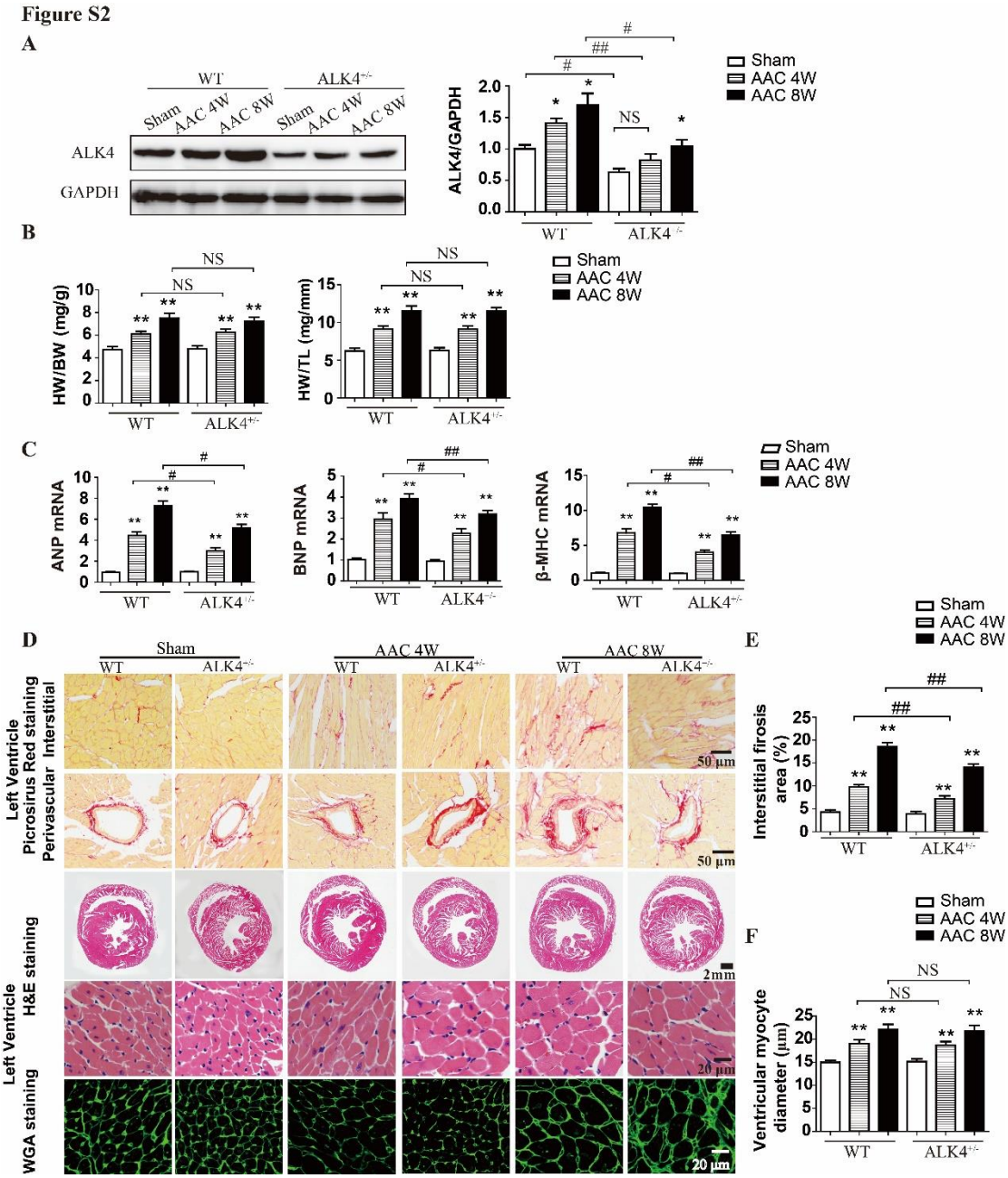

Figure S2. AAC-induced ventricular remodeling in ALK4$^{+/-}$ mice and WT littermates.

(A) Changes in ALK4 protein expression by western blotting in left ventricles of ALK4$^{+/-}$ mice and WT littermates at four or eight weeks post AAC operation (n=5 in each group). (B) Heart weight to body weight ratio (HW/BW) and heart weight to tibia length ratio (HW/TL) of ALK4$^{+/-}$ mice and WT littermates at four or eight weeks post AAC operation (n=8 in each group). (C) mRNA expression of ANP, BNP and β-MHC of left ventricles from ALK4$^{+/-}$ mice and WT littermates post sham or AAC

(n=4 in each group). (D) Representative images of Picrosirius Red, HE and WGA staining of the left ventricle tissues obtained at four or eight weeks post AAC in $ALK4^{+/-}$ mice and WT littermates (n=6 in each group). The scale is marked on the representative images (scale bar, 50 μm for the first and second panel; 2 mm for the third panel; 20 μm for the fourth and fifth panel). Quantification of (E) the left ventricular interstitial fibrosis (n=6 in each group, ≥40 fields per group) and (F) the left ventricular myocyte cross-sectional area based on WGA staining (n=6 in each group, ≥100 cells per group) in $ALK4^{+/-}$ mice and WT littermates between sham or AAC groups. Data were presented as mean ± SEM. $^{*}p < 0.05$, $^{**}p < 0.01$ vs corresponding sham group. $^{\#}p < 0.05$, $^{\#\#}p < 0.01$ vs corresponding WT group. NS, not significant. AAC, abdominal aortic constriction; HW, heart weight; BW, body weight; TL, tibia length; HE, hematoxylin and eosin; WGA, wheat germ agglutinin; ANP, atrial natriuretic peptide; BNP, brain natriuretic peptide; β-MHC, β-myosin heavy chain.

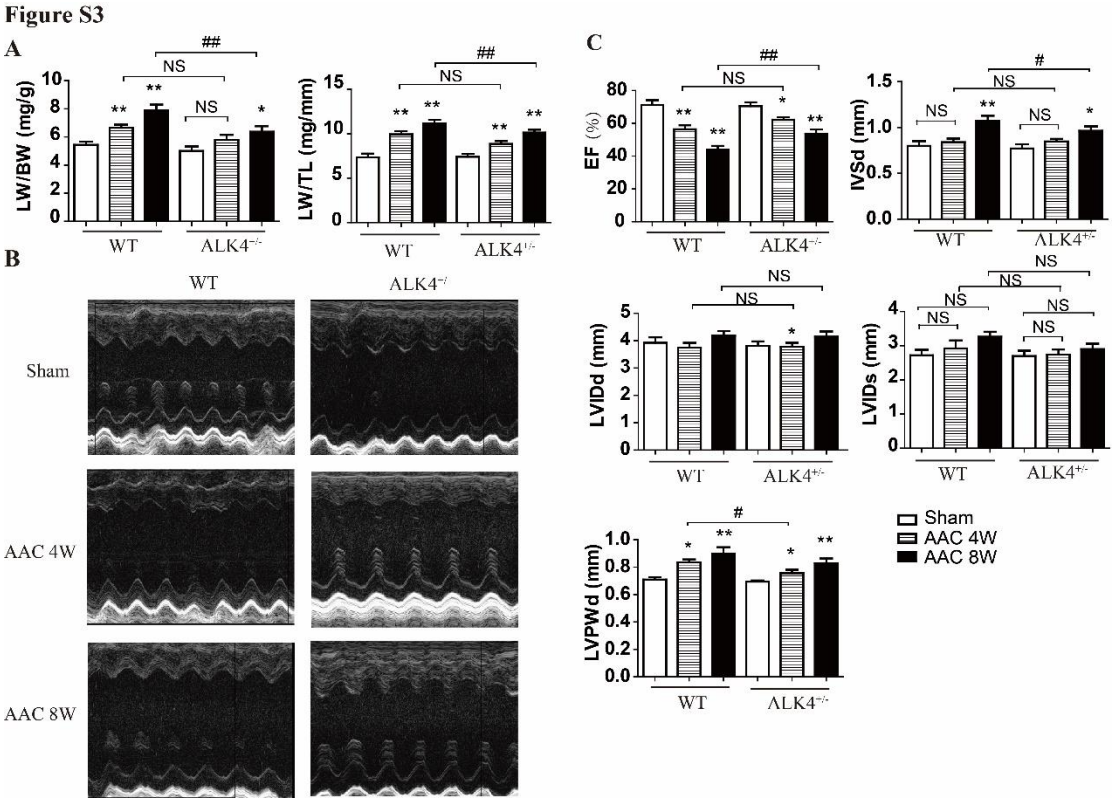

Figure S3. Haplodeficient ALK4 attenuates AAC-induced cardiac dysfunction.

(A) Lung weight to body weight ratio (LW/BW) and lung weight to tibia length ratio (LW/TL) of ALK4$^{+/-}$ mice and WT littermates at four or eight weeks post AAC operation (n=8 in each group). (B) Representative M-mode ventricular echocardiographic images of ALK4$^{+/-}$ mice and WT littermates at four or eight weeks post AAC operation. (C) Quantitative changes in EF, IVSd, LVIDd, LVIDs and LVPWd were compared between two genotypes at four or eight weeks post AAC (n=5 in each group). Data were presented as mean±SEM. $^{*}p < 0.05$, $^{**}p < 0.01$ vs corresponding sham group. $^{\#}p < 0.05$, $^{\#\#}p < 0.01$ vs corresponding WT group. NS, not significant; LW, lung weight; BW, body weight; TL, tibia length; AAC, abdominal aortic constriction; EF, ejection fraction; IVSd, diastolic interventricular septum; LVIDd, diastolic left ventricular internal diameter; LVIDs, systolic left ventricular internal diameter; LVPWd, diastolic left ventricular posterior wall.

Figure S4

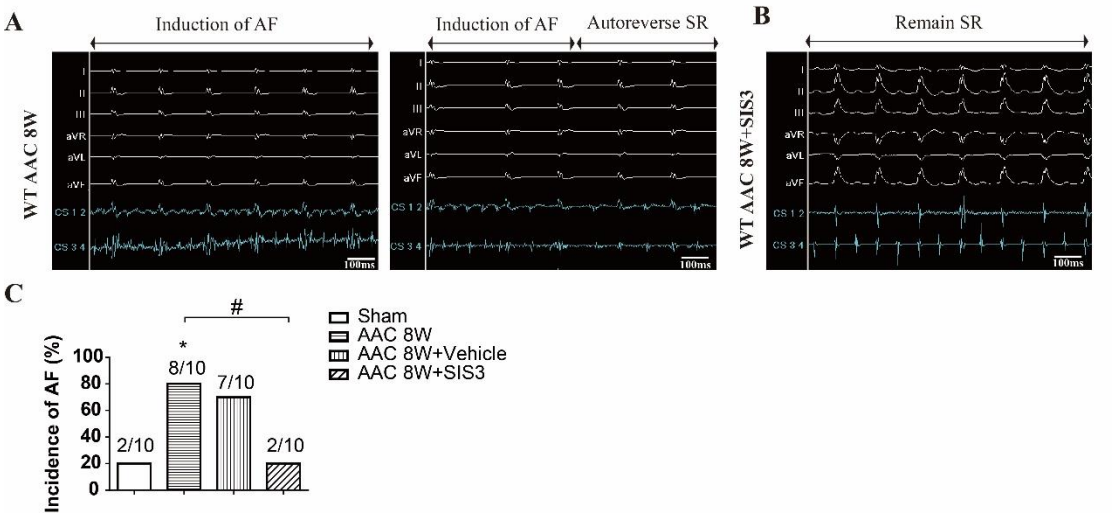

Figure S4. Osmotic mini-pump implantation of smad3 inhibitor SIS3 inhibited the vulnerability of AF at eight weeks post AAC.

(A-B) Example electrical tracings of surface and intracardiac leads from (A) WT littermates post AAC and (B) WT littermates post AAC with subcutaneously infused with smad3 inhibitor SIS3 (2.5 mg/kg/d) during electrophysiological studies with cycle length of 30 ms. Scale, 100 ms. (C) Number of AF-episodes during the electrophysiological studies (n=10 in each group). Data were presented as mean±SEM. $^{*}p < 0.05$, $^{**}p < 0.01$ vs corresponding sham group. $^{\#}p < 0.05$, $^{\#\#}p < 0.01$ vs corresponding AAC group.